Slow transcriptional elongation causes embryonic lethality and perturbs kinetic coupling of long neural genes

Magdalena M. Maslon[1], Ulrich Braunchsweig[2], Stuart Aitken[1], Abigail R. Wilson[1], Fiona Kilanowski[1], Chris Hunter[1], Benjamin J. Blencowe[2], Alberto R. Kornblihtt[3], Ian R. Adams[1] & Javier F. Cáceres[1]

[1]MRC Human Genetics Unit, Institute of Genetics and Molecular Medicine, University of Edinburgh, UK; [2]Donnelly Centre, University of Toronto, Ontario M5S 3E1, Canada; [3]Instituto de Fisiología, Biología Molecular y Neurociencias (IFIBYNE-UBA-CONICET) and Departamento de Fisiología, Biología Molecular y Celular, Facultad de Ciencias Exactas y Naturales, Universidad de Buenos Aires, Ciudad Universitaria, C1428EHA Buenos Aires, Argentina.

[*]Correspondence should be addressed to I.A. (Ian.Adams.@igmm.ed.ac.uk) or J.F.C. (Javier.Caceres@igmm.ed.ac.uk)

Running title: RNAPII elongation rate and co-transcriptional splicing during development

Alternative splicing (AS) is a highly regulated process that increases protein diversity and is critical for cell differentiation and development. The rate of RNA Polymerase II (RNAPII) elongation has an important role in the control of AS. We generated mouse embryonic stem cells (ESCs) knocked-in for a slow elongating form of RNAPII and show that a reduced transcriptional elongation rate causes early embryonic lethality in mice and impairs the differentiation of ESCs into the neural lineage. The reduced elongation rate caused changes in splicing and in gene expression in ESCs and along the pathway of neuronal differentiation. In particular, we found a crucial role for RNAPII elongation rate in transcription and splicing of long neuronal genes involved in synapse signaling. The impact of the kinetic coupling of RNAPII elongation rate with AS is more predominant in ESC-differentiated neurons than in pluripotent cells. Our results demonstrate the requirement for an appropriate transcriptional elongation rate to ensure proper gene expression and to regulate AS during development.

[*Keywords*: RNAPII; transcription elongation rate; co-transcriptional splicing; kinetic coupling; mouse model, ESCs differentiation, neurons]

Supplemental material is available for this article.

Alternative splicing (AS) is a highly regulated process that generates RNA diversity and is a major contributor to protein isoform diversity. Its regulation not only depends on the interaction of trans-acting factors with regulatory RNA cis-acting sequences but also on multiple layers of regulation, including DNA methylation, chromatin structure and modification, and transcription (Schwartz and Ast 2010; Lev Maor et al. 2015; Naftelberg et al. 2015). The co-transcriptional nature of pre-mRNA splicing together with functional links between components of the transcription and splicing machineries led to the suggestion that the rate of transcription elongation acts to control AS in mammalian cells (Beyer and Osheim 1988; Roberts et al. 1998; Pandya-Jones and Black 2009). The splicing factors TCERG1/CA150 (Suñé and Garcia-Blanco 1999; Sanchez-Alvarez et al. 2006) and SRSF2 (Lin et al. 2008) have been reported to stimulate transcriptional elongation. A role for Transcription rate also influences splicing fidelity and co-transcriptionality in budding yeast (Aitken et al. 2011; Aslanzadeh et al. 2018; Herzel et al. 2017).

Recent studies revisited the contribution of the kinetics of RNA polymerase II (RNAPII) elongation to the regulation of AS, giving rise to two complementary models (Bentley 2014; Naftelberg et al. 2015). The “window of opportunity” or kinetic model of AS regulation proposes that the rate of RNAPII elongation influences the outcome of AS selection. Use of a mutant form of RNAPII (C4/R749H), with a slower elongation rate leads to an increased (de la Mata et al. 2003) or decreased (Dujardin et al. 2014) inclusion of alternative cassette exons into mature mRNA. A complementary model, termed ‘Goldilocks’, concluded based on the study of RNAPII mutants with both slow and fast elongation rates, that an optimal rate of transcriptional elongation is required for normal co-transcriptional pre-mRNA splicing (Fong et al. 2014). In both models, recruitment of splicing regulators to cis-

acting RNA sequences, as well as nascent RNA folding are influenced by the elongation rate of RNAPII (Eperon et al. 1988; Buratti and Baralle 2004; Saldi et al. 2018). The global impact of RNAPII elongation rate in the regulation of AS was confirmed by perturbing RNAPII elongation with the use of drugs that inhibit Pol II elongation (Ip et al. 2011). Exogenous agents also affect transcriptional coupling to AS. For instance, UV irradiation promotes RNAPII hyperphosphorylation with the subsequent inhibition of transcriptional elongation, leading to changes in AS, suggesting that transcriptional coupling to AS is a key feature of the DNA-damage response (Muñoz et al. 2009; Williamson et al. 2017). So far, all studies in mammalian systems investigating the link between transcription elongation and AS have been confined to the use of cultured cells transfected with an α-amanitin-resistant slow or fast elongating RNAPII. The consequences of this mechanism of regulation *in vivo* remain unexplored.

Here, we sought to address how does an altered transcriptional elongation rate affect gene expression and the control of AS? Secondly, what are the extent and the phenotypic consequences of the elongation control of AS? We generated mouse embryonic stem cells (ESCs) knocked-in for a slow RNAPII mutant allele (C4/R749H). We show that an appropriate RNAPII elongation rate is essential for proper mouse development. We observed that a reduced elongation rate results in major changes in splicing and in gene expression in pluripotent ESCs and along the pathway of neuronal differentiation. The impact of the kinetic coupling of RNAPII elongation rate with AS is more predominant in ESC-differentiated neurons than in pluripotent cells, as it is essential for the expression and splicing of neuron-specific genes involved in synapse signaling.

Results

Generation of slow RNAPII knock-in mutant mouse ES cells

To address the consequences of an altered transcriptional elongation rate for gene expression and for the kinetic control of AS, we set out to generate an *in vivo* model of a slow RNAPII by introducing a R749H mutation into the endogenous *Pol2ra* in mouse ESCs. This mutation is equivalent to the C4 point mutation identified in the *Drosophila* pol II largest subunit, which confers a lower elongation rate, is less capable of transcribing through natural elongation blocks, and causes non-lethal developmental defects in the heterozygous state (Coulter and Greenleaf 1985; Mortin et al. 1988; Chen et al. 1996). The targeting in mouse ESCs was achieved by successive homologous recombination of constructs that contained a large portion of DNA encoding mouse RNAPII, including exon 14 harboring the R749H mutation (**Fig. 1**, henceforth referred to as WT/slow and slow/slow ESCs). We confirmed the correct targeting by Southern blotting (**Supplementary Fig. 1a**) and Ion Torrent sequencing over a few kb region around the R749H mutation (data not shown). We verified the expression of mutant RNAPII in these cells by cDNA sequencing, a diagnostic *Xho*I digest (**Fig. 1b,c**), and by allele-specific RT-qPCR (**Supplementary Fig. 1b**).

Slow transcription elongation hinders early mouse development

The mutant ESCs were used to generate a slow RNAPII knock-in mouse model. First, we obtained mouse chimaeras from WT/slow ESCs clones; however, no germline transmission was observed following repeated attempts of breeding 8 chimeric male animals (data not shown). This indicates that ESCs with a heterozygous slow RNAPII are not able to contribute to gametogenesis. As an alternative approach, we set out to

generate R749H mutant mice using CRISPR/Cas9 (**Fig. 2a**). Specific single guide RNAs (sgRNAs) against *Pol2ra* were used for microinjection along with the Cas9 mRNA and a repair oligonucleotide template containing the R749H mutation ("slow oligo") and subsequently embryos were transferred into recipient mice at the two-cell stage. No live-borne mice were obtained containing homozygous or even heterozygous mutations in the *Polr2a* locus among the 47 pups (**Supplementary Fig. 2**). To rule out inefficient induction of double-strand DNA breaks (DSBs) by sgRNAs, we co-injected the same pair of sgRNAs with a repair template mixture containing a 1:1 ratio of a slow and a silent oligo, the latter being a repair template containing silent mutations. Again, we could not detect the slow mutation in any of the 51 pups born; however, we obtained two homozygotes and four heterozygotes through repair with silent oligo (**Fig. 2b, Supplementary Fig. 2**). Next, we investigated at what stage this mutation caused embryonic lethality. We microinjected slow oligo along with guide RNAs and analyzed the resulting embryos at the late morula/blastocyst stage. We found several slow heterozygous and 1 homozygous embryos, revealing that the R749H mutation was tolerated at the pre-implantation stage (**Fig. 2b, Supplementary Fig. 2**). However, only one heterozygous and no homozygous slow mutations were found in mid-gestation embryos at E9.5-E11.5. Thus, we conclude that the *Polr2A* R749H mutation causes early embryonic lethality.

The R749H mutation decreases the transcription elongation rate in mouse ESCs

We analyzed the effect of the slow RNAPII mutation in ESCs using 5,6-dichlorobenzimidazole 1-beta-D-ribofuranoside (DRB) to measure RNAPII transcriptional elongation rates (Singh and Padgett 2009). DRB inhibits P-TEFb–dependent phosphorylation of the transcription elongation factor Spt5 and of Serine 2

in the carboxy-terminal domain (CTD) of RNAPII. Thus, newly initiated RNAPII cannot progress to the elongation phase; however, upon DRB removal, all initiated polymerases are released and the appearance of selected intron-exon junctions can be monitored by qRT-PCR in a time-dependent manner. We monitored how transcription proceeded through the *Utrophin* and *Itpr1* genes, following DRB removal. Transcription over the first exon-intron junctions did not differ between the wild-type (WT) and mutant cell lines (**Supplementary Fig. 3a**, Exon 1-Intron 1 panel). However, appreciable pre-mRNA levels at the more downstream exon-intron junctions were detected earlier in WT than in slow/slow cells. For example, the appearance of an exon-intron junction 133kb downstream from the *Itpr1* transcription start site was detected at 40 min post-DRB release for the WT, as compared to 90 min for the mutant RNAPII (Supplementary **Fig. 3A**, Exon 5-Intron 5 panel). An overall mean elongation rate across *Utrophin* and *ITPR1* was estimated to be 5.6 and 3.3 kb/min, respectively in WT cells, as compared to 1 and 1.5 kb/min in slow/slow cells. We also measured overall transcription using a reversible DRB block followed by incubation with medium containing tritiated (3H)-Uridine. Time-resolved accumulation of newly made RNA, as measured by the incorporation of 3H-Uridine, was attenuated in slow/slow in comparison to WT ESCs (**Supplementary Fig. 3b**). We also found that nuclear extracts isolated from slow/slow cells were less efficient in driving the production of a run-off transcript from the artificial DNA template (**Supplementary Fig. 3c**). These results are in agreement with the previous observation that the R749H mutation in RNAPII leads to decrease in the transcription elongation rate *in vitro* (Boireau et al. 2007) and that the elongation rate positively correlates with expression levels (Danko et al. 2013; Jonkers et al. 2014).

We analyzed RNAPII elongation rates genome-wide using metabolic labeling of newly transcribed RNAs by the uridine analogue, 4-thiouridine (4sU)(Rädle et al. 2013; Fuchs et al. 2014). Transcription was arrested with DRB for 4 hours, following DRB removal, cells were allowed to transcribe for 5 and 15 mins. To label the newly transcribed RNA, cells were pulsed with 4sU for the last 10 min of each time point (**Fig. 3a**). Cells not released from transcriptional block ("0 min") were also labeled with 4sU. Following biotinylation and purification, 4sU-labeled RNAs was subjected to deep sequencing. At time "0 min" the vast majority of reads were observed over a narrow area near the promoter (**Fig. 3b**, black line, **Supplementary Fig. 4a**, top panel). As time progresses, the reads from nascent RNA are observed further into the gene bodies, referred to as the transcription "wave front" progression (**Supplementary Fig. 4a,** wave front progression in *Notch1*). On average, we observed that in WT cells, RNAPII had progressed 11 kb into the gene at 5 min and up to 35.8 kb at 15 min after DRB removal. By contrast, in slow/slow cells the transcription wave-fronts reached 8.6 kb and 26.7 kb at 5 and 15 min time points, respectively (**Supplementary Fig. 4b** and **Fig. 3b**). Genome-wide, we observed an average elongation rate of 2,450 bases/min in WT cells, but reduced rates of 1,780 bases/min in slow/slow cells (**Fig. 3b,d**). The density plot of elongation rates demonstrates that the dynamic range of transcription rates is narrower in slow RNAPII cells, whilst in WT cells it is bimodal revealing a population of RNAPII transcribing at higher rates (**Fig. 3c**). Indeed, most genes have a lower elongation rate in slow/slow cells in comparison to wild-type cells (e.g. *Ern1* is transcribed at 4.2kb/min and 1.9kb/min, in WT and slow/slow cells, respectively). Interestingly, there are examples of genes that are transcribed faster in slow/slow cells. A slower elongation rate might translate to a longer residence time, allowing more time for

positive factors to bind and/or stimulate RNAPII and consequently lead to higher transcription rates for these genes. Finally, there is a positive correlation between elongation rate and expression levels (Supplemental Fig. S4C), indicating that on average, highly expressed genes have faster elongation rates in agreement with previous reports (Jonkers et al. 2014; Danko et al. 2013). Overall, these data validate previous results obtained in cultured cells transfected with an α-amanitin-resistant RNAPII harboring the C4 mutation (de la Mata et al. 2003; Fong et al. 2014) and confirm that the endogenous knock-in of a slow RNAPII mutation affects negatively the transcriptional elongation rate in mouse ESCs.

Role of transcriptional elongation during neural differentiation

To assess whether a differential transcription elongation rate affects ESC differentiation, we exploited an *in vitro* model of neuronal development. During embryonic development, different pathways control self-renewal and differentiation capacity of neural progenitors (Doe 2008; Aguirre et al. 2010; Faigle and Song 2013). We used a serum-free adherent monolayer culture protocol (Ying et al. 2003; Conti et al. 2005), that generates multipotent Sox1 and nestin-positive neuronal progenitor cells (NPCs) (**Fig. 4a**). The ESC-derived NPCs can then be used to generate neural stem cells (NSCs) by allowing these cells to form floating aggregates in epidermal/fibroblast growth factor 2 (EGF/FGF2)-containing medium that then outgrow a population of bipolar NSCs when plated in adherent conditions (**Fig. 4a**). The initial heterogeneity of NSC-containing cell population is reduced following a few passages. Alternatively, the ESC-derived NPCs can be differentiated into all three neural lineages. For example, when cultured adherently on poly-ornithine/laminin in

media containing cAMP and ascorbic acid, NPCs differentiate into Tuj1+ immature neuronal cells and further into Map2-positive mature post-mitotic neurons.

We first attempted to differentiate WT ESCs and slow/slow ESCs into NPCs; however, we observed decreased proliferation or compromised differentiation potential of slow/slow cells. Nevertheless, we found that both wild-type and slow/slow cells generated Sox1 and nestin-positive NPCs (**Fig. 4b**). Neuronal differentiation becomes evident at around the fifth day of adherent monoculture, and indeed following 7 days we observed Tuj1-positive cells in both WT and slow/slow cells. Overall, we conclude that slow allele is compatible with *in vitro* differentiation into NPCs. We next tested if we could generate NSCs from slow/slow ESC-derived NPCs. Interestingly, we found that despite obtaining neural aggregates, slow/slow NSCs could not be maintained in EGF/FGF2 proliferating conditions (**Fig. 4d** and data not shown). Instead, following a few passages we noted the appearance of flattened differentiated cells in the slow/slow cultures, and subsequently we observed overwhelming cellular death. Strikingly, amongst some of the remaining nestin-positive slow/slow cells, we observed promiscuous differentiation to Tuj1+ cells (**Fig. 4d**). These results suggest that the balance between the self-renewing cell state and differentiation is perturbed in slow/slow NSCs.

Although the slow RNAPII allele appears to impair the maintenance of NSCs, the presence of differentiated Tuj1 neurons in both the monolayer (**Fig. 4b**) and the NSC cultures (**Fig. 4d**) suggests that a slow transcriptional elongation rate does not impair neuronal differentiation per se. Indeed, WT and slow/slow ESCs generated PSA-NCAM-positive neuronal precursors with similar efficiencies in this protocol (data not shown) and differentiated into immature Tuj1-positive and mature Map2-positive neurons (**Fig. 4e**). Whereas we observed a robust expression of the synaptic marker

(Syn1) in WT neurons, it seemed greatly reduced in slow/slow neurons (**Fig. 4e**, right panel). Overall these data show that the slow mutation in RNAPII causes problems in the maintenance/self-renewal of NSCs and appears not to interfere with neuronal differentiation *per se;* however, it also indicates that homozygous slow neurons might be functionally or developmentally different than WT neurons.

Transcriptional elongation rate influences AS decisions in ESCs and during neural differentiation

Next, we investigated AS changes by RNA sequencing (RNA-seq) analysis of poly(A)+ RNA isolated from pluripotent ESCs, NPCs, PSA-NCAM+ cells and neurons (**Fig. 5a**, **Supplementary Table 1**). We identified 80, 171, 50 and 424 events of enhanced exon inclusion, comprising cassette exons and microexons, in slow/slow ESCs, NPCs, PSA-NCAM+ cells and neurons, respectively, as compared to their WT counterparts. We also observed that whereas exon events did not show a bias towards increased inclusion in slow/slow ESCs or NPC cells when compared to WT cells, there was some tendency for an increased exon inclusion in slow/slow neurons (60% of alternative events are more included) (**Fig. 5a**). By contrast, we found that exon skipping was enhanced relative to inclusion by the slow RNAPII mutant, with 94, 524 and 148 skipped cassette exons and microexons detected in ESCs, NPCs and PSA-NCAM+ cells, respectively. This is compatible with the current models of kinetic coupling, where a slow RNAPII can lead to enhanced exon inclusion if the AS event depends on the recruitment of positive regulators, or to exon skipping, if splicing inhibitors are recruited (Dujardin et al. 2014). Indeed, as an example of the latter, RNA maps produced for RNA-binding proteins (CISBP-RNA IUPAC binding motifs (Ray et al. 2013)) revealed that introns downstream of downregulated exons in

neurons are enriched for Nova and Fox1 binding site (**Supplementary Fig. 5**). Binding of these factors downstream of alternative exons, has been previously shown to increase their skipping (Ule et al. 2006; Licatalosi et al. 2008; Zhang et al. 2008).

Importantly, the extent of splicing changes was much more pronounced in NPCs and fully differentiated neurons in comparison to ESCs (174 cassette exon and microexon events changing in slow/slow ESCs as compared to 695 or 704 cassette exons and microexons changes observed in slow/slow NPCs and neurons, respectively, **Fig. 5a**). These results underscore the predominant role of kinetic coupling as differentiation progress. A possible explanation for this observation is related to changes in chromatin structure during cell differentiation. Chromatin is reported to be more open and accessible in pluripotent ESCs (Gaspar-Maia et al. 2011). This differential chromatin organization will likely have a direct influence in the elongation rate of RNAPII (Selth et al. 2010; Naftelberg et al. 2015). Thus, a slow elongating RNAPII will exacerbate the dependence of AS on kinetic coupling upon cellular differentiation, as it is further hindered by the compactness of chromatin. Not only, did we observe an elevated number of affected exons in slow/slow neurons in comparison to slow/slow ESC, but also the number of splicing changes increases during differentiation to neurons, with 1,365 AS events detected in WT cells upon differentiation, whereas this number increases to 2,252 exons in slow/slow cells (**Supplementary Table 1**). We examined the properties of elongation-rate sensitive exons, namely 5' and 3' splice sites strength, as well as the length of flanking introns and alternative exons (Yeo and Burge 2004; Corvelo et al. 2010; Corioni et al. 2011) (**Fig. 5c** and **Supplementary Tables 2-5).** We noted that exons more included in slow/slow ESCs had longer flanking introns (median of 2,335 and 1,546 bases in included and not-affected exons, respectively). Consistent with the 'window-of-

opportunity' model of kinetic coupling, these longer introns could contribute to a time delay significant enough to promote recognition and splicing of suboptimal exons in nascent transcripts. By contrast, exons skipped in slow/slow neurons were on average shorter and had longer introns, whereas included exons were on average flanked by shorter introns. The features that we identified in neuron-specific exons are similar to those found in exons excluded by a slow RNAPII in 293T cells (Fong et al. 2014).

A reduced transcriptional elongation drives AS independent of gene expression changes

We investigated differential gene expression between WT and slow/slow pluripotent ESCs, NPCs, PSA-NCAM+ cells and neurons. High-throughput RNA-seq of poly(A)+RNA revealed changes in the expression of several hundreds of genes in slow/slow cells, as compared to their WT counterparts (**Fig. 6a, b**, **Supplementary Table 6**). We looked at whether the observed changes in AS are coupled to changes in the expression of corresponding genes. Notably, the differential splicing observed in the presence of a slow elongating RNAPII is generally not driven by differential gene expression (**Supplementary Fig. 6**). The exception is some cases of intron retention, where negative correlation with the expression might reflect frequent coupling of intron retention to NMD (**Supplementary Fig. 6**). We investigated whether the splicing signature in slow/slow cells was a result of perturbations in the elongation rate or was indirect and caused by changes in expression of splicing factors and/or RNA-binding proteins (RBPs). We used available datasets from experimental perturbations of some of differentially expressed splicing factors (**Supplementary Fig. 7a)** and noticed some overlap with the splicing events found in slow/slow cells (**Supplementary Fig. 7b**). They are not, however, sufficient to explain all the changes

that we observe in slow/slow cells, indicating that most changes in AS events can be attributed to a slower elongation rate.

Slow transcription elongation perturbs expression of long synaptic genes

To understand whether slow RNAPII-responsive genes are functionally linked, and whether certain pathways were particularly sensitive to kinetic coupling, we searched for significant enrichment of specific Gene Ontology (GO) terms in all stages of differentiation (**Supplementary Fig. 8** and data not shown). We first noted that genes upregulated in NPCs are involved in neuronal functions (**Supplementary Fig. 8A**), which might explain the phenotypes observed in slow/slow NSCs (**Fig. 4**). Indeed, we confirmed upregulation of *Nr2f1*, *Nr6a1, Ascl1 and Crabp2* genes. Their overexpression has been shown to suppress proliferation of progenitor cells, induce neurogenesis and neuronal maturation (Gkikas et al. 2017; Chanda et al. 2014). (**Supplementary Fig. 9**) and could explain the premature differentiation observed in slow/slow NSCs. In parallel, we observed that the EGF receptor (EGFR) was two-fold downregulated in slow/slow NPCs (**Supplementary Table 6**). As EGF withdrawal causes massive cell death and premature differentiation of NSCs (Conti et al. 2005), decreased expression of EGFR in slow/slow NSCs could contribute to the observed lack of their self-renewal in EGF/FGF2 proliferating conditions. Enrichment Map visualization of gene-sets enriched amongst downregulated and AS genes in slow/slow neurons revealed that they are involved in synapse formation and synaptic signaling (**Fig. 7a, c** and **Supplementary Fig. 8b-d**). Indeed, genes downregulated in slow/slow neurons encoded proteins involved in the entire life cycle of synaptic vesicles. Amongst them were: Syn1 and Syn2, which tether the vesicle to the actin cytoskeleton (Thomas et al. 1988), Snap25, Stx1b, Stxbp1, Syt1 proteins that are

involved in synaptic vesicle fusion and recycling; as well as neurexins (NRXN1 and NRXN2) and contactin-associated proteins (CNTNAP2 and CNTNAP3) that form the synaptic scaffolding system and are involved in trans-synaptic communication.

The largest differences observed in AS in slow/slow neurons involved skipping of exons that have been previously shown to be included in neurons, and conversely most exons that are included in slow/slow neurons, are normally skipped in neurons (**Fig. 7b**)(Irimia et al. 2014). Moreover, and similarly to downregulated genes, these alternative events involved proteins that are important for synaptic signaling (**Fig. 7a, c**, **Table 1** and **Supplementary Table 7**). For example, we observed increased skipping of the alternative exon in *Scrib*, a gene encoding a protein involved in neurotransmitter release (**Fig. 5b** and **7c**). We also confirmed differential splicing of Apbb2, a protein involved in synaptic vesicle loading (**Fig. 5b** and **7c**). We noted altered splicing amongst members of neurexins, synaptic receptors that undergo an extensive combinatorial use of AS to provide molecular diversity required for the functional differentiation of synapses (Schreiner et al. 2014). (**Supplementary Table 1**). Finally, we observed, AS events in proteins involved in the synaptic vesicle cycle, including both pre-synaptic and post-synaptic space, amongst them Stx4A, Syn1, Synj1, Stx3 and many others, some of them resulting in premature termination codons, others changing domain structures or affecting ion transfer, hence all likely contributing to the function of the synapse (**Fig. 7c** and **Table 1**).

Interestingly, we noticed that those genes that are preferentially downregulated and/or alternatively spliced in slow/slow neurons, tend to be significantly longer than those that were not affected or that are upregulated. These include genes encoding proteins present in the synaptic network (**Fig. 7d**). By contrast, we found no significant change in the average gene length between downregulated genes and all

expressed genes in ESCs and PSA-NCAM+ or NPCs (**Fig. 7d** and data not shown). Notably, a slow transcriptional elongation rate reduced expression of nearly all long genes in neurons, with the percentage of downregulated genes in slow/slow neurons progressively increasing from around 40% for 10 kb genes to over 80% for extremely long genes (**Fig. 7e**). Some examples of such genes include *Cntnap2* (2.25 Mb) and *Nrxn1* (1.05 Mb) (**Supplementary Table 6**). Similarly, AS also affected longer pre-mRNAs. From this we speculate that an optimal elongation rate is important to sustain transcription and splicing of particularly long transcripts that are required for neuronal function. Indeed, recent reports propose that long genes require special mechanisms to specifically maintain long-distance transcription. As an example, the neuronal RBP Sfpq (proline/glutamine-rich), has been shown to be a critical factor for maintaining transcriptional elongation of long genes (Patton et al. 1993; Takeuchi et al. 2018). Thus, both downregulated as well as preferentially alternatively spliced genes in slow/slow neurons converged onto long genes that are involved in synaptic function. Candidate genes involved in neurodevelopmental diseases encode synapse proteins and are exceptionally long (Bourgeron 2015). Therefore, we further analyzed the overlap of the genes downregulated and differentially spliced in slow/slow neurons with available datasets for brain disease, including causative genes for autism (SFARI) and schizophrenia. We noted that these genes significantly overlapped with those linked to neurological disorders, including ASD disease (**Supplementary Table 8**). From these experiments, we conclude that a reduced transcriptional elongation rate preferentially affects the expression and AS of long synaptic genes.

In summary, the development of a genetic system based on knock-in for a slow RNAPII mutation in mouse ESCs unequivocally established that an appropriate RNAPII elongation rate is essential for proper mouse development and for gene

expression and its kinetic coupling with AS. Our results provide compelling evidence that transcription elongation rates have a regulatory role in the expression of genes and the regulation of their AS patterns during development.

Discussion

We observed that a slow transcriptional elongation rate resulted in early embryonic lethality even in heterozygosity (**Fig. 2**). It is possible that a slow elongation rate cannot sustain the high levels of mRNA production required at early stages of development (Koh et al. 2015; Percharde et al. 2017). Similarly, loss of self-renewal in slow/slow NSCs could be related to the inability of cells harboring a slow RNAPII to maintain the required levels of transcriptional output. Initial stages of mouse embryonic development display a great range of cell cycle duration, from up to 20 hours for the first cell division to 2-3 hours cell cycles during gastrulation (Artus et al. 2006) or 8 hours during initial stages of murine neurogenesis (Takahashi et al. 1995). Thus, a reduced elongation rate in slow/slow mutant embryos might not allow efficient transcription or might delay expression of some crucial mRNAs that need to be expressed in these fast dividing cells. Whereas in mice both the homozygous and heterozygous slow mutation result in embryonic lethality (**Fig. 2**), the C4 mutation in *Drosophila* is tolerated in heterozygosity where the flies present a mutant phenotype called "Ubx effect" that resembles the one seen in flies haploinsufficient for the Ubx protein. This was attributed to Ubx missplicing as it is one of the few *Drosophila* genes with an extremely long intron (50 kb)(de la Mata et al. 2003). This is in agreement with results presented here showing that mouse genes with long introns are preferentially affected by a slow RNAPII in ESC-differentiated neurons.

The slow RNAPII mutant used in this study is less efficient at dealing with naturally occurring pause sites *in vivo* (de la Mata et al. 2003; Fong et al. 2014). We found that the impact of RNAPII elongation rate on AS is predominant in ESCs-differentiated NPCs and neurons. This is likely caused by distinct chromatin environment between pluripotent and differentiated cells having a differential impact on RNAPII transcriptional elongation rate. While chromatin is quite dispersed in E3.5, heterochromatin foci appear in E5.5, which corresponds to the epiblast stage following embryo implantation (Ahmed et al. 2010). Indeed, despite the conflicting literature regarding deposition of histone marks throughout differentiation (Azuara et al. 2006; Wen et al. 2009; Lienert et al. 2011), a large body of evidence suggests that chromatin undergoes dynamic changes during differentiation leading to a more compact environment in the differentiated state. Various mechanisms might promote the switch from a more open to a more close chromatin during cell differentiation, including an increase in repressive histone marks, a local change in nucleosome occupancy, or a general increase in histones levels (Fiszbein et al. 2016; Gavin et al. 2017; Yoon et al. 2018). Indeed, the nuclei of ESCs macroscopically appears to contain less condensed chromatin, whereas well-defined foci of compact heterochromatin become evident in ESCs-derived NPCs (Meshorer et al. 2006). Indeed, chromatin structure can become a major impediment to transcriptional elongation and histone modifications can directly affect the nucleosomes, by either loosening or tightening DNA binding around them (Veloso et al. 2014; Jonkers and Lis 2015). Moreover, exons have a negative effect on RNAPII elongation rate, which could be associated with exonic features, such as a higher CG content, and exon-specific histone marks (H3K36me3 and H3K4me1)(Jonkers et al. 2014). An example of a crosstalk between the chromatin environment an AS has been shown in the case

of exon18 in the neural cell adhesion molecule (NCAM), where membrane depolarization of neuronal cells induces a local H3K9 hyperacetylation, resulting in exon skipping (Schor et al. 2009). Conversely, inducing a more compact chromatin state by transfection of siRNAs targeting the intron downstream of an alternative exon, promotes H3K9 and H3K27 methylation, HP1 recruitment, in turn leading to local roadblocks for RNAPII elongation rate and increased kinetic coupling(Alló et al. 2009). We speculate that the specific changes in chromatin structure during differentiation might create natural "roadblocks"to elongating RNAPII, which is further enhanced in slow RNAPII-expressing cells leading to increased kinetic coupling observed in NPCs and neurons derived from slow/slow cells.

Slow RNAPII leads to specific downregulation of longer genes in neurons. Dysregulation of the expression of these long genes might represent a mechanism underlying neurodegenerative and psychiatric disorders (Gabel et al. 2015; King et al. 2013). For example, loss of FUS/TLS and TDP43, genes linked to ALS, preferentially affects splicing of long pre-mRNAs (Lagier-Tourenne et al. 2012). The neuronal RBP SFPQ, which is required to sustain long-distance transcription elongation for longer genes (Takeuchi et al. 2018), has a role in neurodegenerative diseases, including ALS, ASD and Frontotemporal lobar degeneration (FTLD). The differentially expressed and alternatively spliced pre-mRNAs in neurons, are involved in synapse signaling, neurite outgrowth and axonal guidance (**Fig. 7**). We speculate that mis-regulation of RNAPII elongation rate could have detrimental implication in neurodevelopment, preferentially affecting the expression and/or splicing of synaptic proteins, which are encoded by particularly long genes (**Fig. 7**). Indeed mutations in genes involved in synaptic signaling lead to neurodevelopmental diseases, including Autism spectrum disorder (ASD)(Bourgeron 2015). Importantly, chromatin

remodeling, transcription and splicing genes have been identified in genetics studies of *de novo* mutations in autistic patients (De Rubeis et al. 2014). Physiological conditions that could alter RNAPII elongation or mutations disrupting elongation rate control might affect preferentially the nervous system, as these cells express particularly long genes. This could result not only in changes in transcription but also affect AS patterns via kinetic coupling. These observations highlight an essential role for an appropriate elongation rate in gene expression and splicing regulation during neural development and suggest that its misregulation could underlie some neurological disorders. In conclusion, we show that a slow elongation rate affects gene expression and AS, consistent with the coupling of transcription with splicing. This kinetic control of AS is more strongly affected as differentiation progress. Most notably, we identify elongation rate control as a major mechanism to sustain transcription and splicing of long neuronal genes involved in synapse signaling. This study provides a compelling evidence that transcription elongation rates have a regulatory role in the expression of genes and the regulation of their AS patterns during development.

Methods

Cell lines generation. BAC containing the Polr2a locus was used to introduce the R749H mutation into exon 14. To this end two sets of primers were used that have 50bp homology arms to target the Pol2 exon 14 and either regions to hybridize to galK selection cassette or complementary regions containing the R749H point mutation to hybridize to each other. The galK selection cassette was amplified from pGalK and 1.3kb product was electroporated into *E.coli* strain containing BAC clone bMQ420i24 and recombination was induced by heat shock. PCR was set up with second pair of primers and the resulting 132bp primer dimer was recombined with Gal modified BAC clone. Gal-modification introduces EcoRI and BamHI restriction sites into exon 14 of Polr2a along with R749H. 10.4 kb region of the Polr2a locus was retrieved from the Gal-modified Polr2a BAC clone by gap repair. Mini-targeting cassette was then generated to recombine Frt-flanked neomycin cassette into intron 12 of Polr2 locus. This generated the Pol2ra constitutive targeting vector. The resulting targeting vectors were linearized and introduced into E14 ESCs by electroporation. Genomic DNAs from were screened for homologous recombination by PCR and Southern blot.

Cell differentiation. ESCs were cultured under feeder-free conditions in GMEM medium supplemented with 10% foetal calf serum, NEAA, β-mercaptoethanol, sodium pyruvate, L-glutamine and 100 U/ml recombinant leukaemia inhibitory factor (LIF) on gelatin-coated tissue culture plastic. Before differentiation, cells were freshly defrosted in standard medium and then passaged for 2 passages in 2i medium (1:1 Neurobasal and DMEM/F12, supplemented with 0.5X N2, 0.5x B27, 0.05% BSA,

1μM 0325901, 3μM CHIR99021, 2mM L-glutamine, 0.15mM monothioglycerol, 100U/ml LIF).

Neuroectodermal specification. One day prior to induction of differentiation cells were seeded at high density in 2i medium. The following day, cells were detached using accutase, resuspended in N2B27 media (1:1 Neurobasal and DMEM/F12, supplemented with 0.5X N2, 0.5x B27, 0.1 mM β-mercaptoethanol, 0.2 mM L-glutamine), counted and plated at the appropriated density onto either 15 cm plates or 6 well plates that have been coated with a 0.1% gelatin solution. Culture medium was changed every second day. The differentiation potential is greatly influenced by the initial plating density and was previously established to be optimal at approximately 10,000 cells per cm^2, which is what we observed with the differentiation of WT ESCs. On the contrary, we observed increased cell death at plating densities below 30,000 cells per cm^2 for slow/slow cells, suggesting decreased proliferation or compromised differentiation potential of these cells.

Isolation of *PSA-NCAM+ cells.* For neuronal precursor differentiation, cells were differentiated as above for 10 days, detached using accutase and PSA-NCAM+ cells were purified using PSA-NCAM beads (Miltenyi).

Deriving NS cells. For derivation of neural stem cells at day 7 of differentiation, cultures were detached using accutase, 2-3 x 10^6 cells were re-plated into an uncoated T75 flask in NS expansion media, comprising DMEM/F12 medium supplemented with 2mM L-glutamine, 0.5x N2, B27, glucose, BSA, Hepes and 10ng/ml of both mouse EGF (Peprotech) and human FGF-2 (Peprotech). Within 2-3 days, thousands

of cell aggregates formed in suspension culture and were harvested by centrifugation at 700 rpm for 1 minute. They were then re-plated onto a laminin coated T75 flask. After few days, cell aggregates attached to the flask and outgrew with NS cell.

Differentiation to neurons. For neuronal generation and maturation at day 7 of differentiation, cultures were detached using accutase, replated onto poly-l-ornithine/laminin (100 μg/ml and 10 μg/ml, respectively, Sigma–Aldrich) coated surfaces at 1.5-2 x 10^4 cells/ cm^2 in N2B27 medium containing 0.2mM ascorbic acid and 0.25 mM cAMP. Cells were grown for the additional 7 days, with 80% media exchange every second day.

Nascent transcription assays. Elongation rate experiments were carried out as described (Singh and Padgett 2009). Briefly, cells were treated for 4 hr with 100 μM 5,6-dichlorobenzimidazole 1-β-d-ribofuranoside (DRB) to inhibit transcription. To restart transcription, cells were washed twice in war, PBS, and incubated with fresh medium. During 0-180 min incubation, at indicated times, cells were lysed directly in Trizol and RNA was extracted according to manufacturer's recommendations. 5 μg of Total RNA were reverse transcribed using random hexamers and Superscript III. Pre-mRNA levels were measured by quantitative RT-PCR using Sybr Green Master Mix and Lightcycler 480 (Biorad). Primers used in the quantitative RT-PCR are available on request. Pre-mRNA levels were normalised to pre-mRNA levels at t=0 min. Results depict average of three independent experiments, ± standard error.

Pulse-label transcription assay. Cells were treated for 4 hr with 100 μM 5,6-dichlorobenzimidazole 1-β-d-ribofuranoside (DRB) to inhibit transcription. To restart

transcription, cells were washed twice in war, PBS, and incubated with fresh medium with the addition of mCi/ml [3H]-uridine for 0-30 minutes. Cells were harvested in Trizol and RNA isolated according to manufacturer's instructions. Labeled uridine incorporation was quantified by scintillation counting.

4sU-DRBseq. ESCs were seeded in 15-cm plates in 2i medium. At the 80-90% confluency, cells were treated with 100 μM DRB. Following 4 hours of incubation, DRB-containing media was removed, cells were washed twice with warm PBS and placed in fresh media without DRB. 4-thiouridine (4sU) was added to medium at a final concentration of 1mM for 10 minutes before each harvest. Cells were lysed directly on a plate with 5 ml of Trizol at indicated transcription elongation time point. Total RNA was isolated as per manufacturer's instructions. Total RNA (100–200 μg) was used for biotinylation and purification of 4sU-labeled nascent RNAs. The biotinylation reaction consisted of total RNA and EZ-Link Biotin-HPDP dissolved in dimethylformamide (DMF), and was performed in labeling buffer (10 mM Tris pH 7.4, 1mM EDTA) for 2 hours with rotation at room temperature. Unbound Biotin-HPDP was removed by chloroform/isoamylalcohol (24:1) extraction in MaXtract tubes (Qiagen). RNA was precipitated with 10th volume of 5M NaCl and 1 volume of isopropanol. Following one wash in 80% ethanol, the RNA pellet was left to dry and resuspended in 100 μl RNase-free water. Biotinylated RNA was purified using μMacs Streptavidin kit. Specifically, 100 μl of beads per 100 μg of RNA was incubated with rotation for 15 min, and then washed three times with washing buffer (100 mM Tris pH 7.5, 10 mM EDTA, 1 M NaCl, 0.1% Tween20) at 65°C, followed by three washes at room temperature. RNA was eluted twice using 100 mM DTT and recovered using RNeasy MinElute Cleanup column (Qiagen) according to instructions. cDNA libraries

were prepared using NEB Next Ultra Directional RNA Library Prep Kit according to the manufacturer's instructions. Libraries were pooled and sequenced on an Illumina HiSeq 4000 system. All reads were aligned to the mouse reference genome (mm10) using bowtie 2 aligner (Langmead et al. 2009) and only those reads that mapped uniquely to the genome, but not to rRNA, were considered. A genome-wide binned profile of the nascent RNA and the transcription wave end were determined using previously developed methods and published software (Fuchs et al. 2015, 2014).

RNA-Seq analysis. RNA-Seq libraries were generated from Poly(A)$^+$ mRNA and sequenced using the Illumina Hi-Seq 2500 or 4000 machine to generate 125 bases or 75 bases, paired end reads, respectively. Reads were mapped to the mouse (mm9) genome. AS analysis of RNA-Seq data was performed with *vast-tools* version 1 (Tapial et al. 2017). From the primary output, events with poor coverage or junction balance were filtered out (vast-tools quality score 3 other than SOK/OK/LOW for cassette exon [CE], microexon [MIC], and alternative 5´ or 3´ splice site [Alt5/3] events or coverage less than 15 reads for intron retention [IR] events; score 4 other than OK/B1 for CE and MIC events and score 5 of less than 0.05 for IR events). Differential AS was scored using vast-tool's diff module requiring $p(|dPSI| > 0) > 0.05$ and a point estimate of $|dPSI| > 10$. Gene expression was analysed based on raw read counts per gene from *vast-tools* using the glm stream of the R package edgeR. Genes with an FDR < 0.05 were considered differentially expressed.

Analysis of splicing factors regulation of AS. We used available RNA-seq data from splicing factor knockdowns or knockouts (MBNL2 in mouse hippocampi (Goodwin et al. 2015; Charizanis et al. 2012), MBNL3 (Poulos et al. 2013) Srrm4/nSR100 and Ptbp1 in mouse N2A cells (Raj et al. 2014), Ptbp2 in mouse brain

(Li et al. 2014), HNRNPA2B1 in mouse spinal cord (Martinez et al. 2016), KHDRSB3 (Ehrmann et al. 2013), Nova1 (Zhang et al. 2010; Ule et al. 2006) and Rbfox1 in mouse whole brain (Lovci et al. 2013)) and their associated controls, to identify AS exons whose inclusion levels are affected by experimental manipulation of the expression of the splicing factors.

***In vitro* transcription assay.** Nuclear extracts were prepared according as previously described (Folco et al. 2012). A DNA construct, containing CMV promoter and encoding β−globin was linearized by restriction digest. *In vitro* transcription reactions were performed at 30°C in 25 µl reaction mixtures containing 375 ng DNA template, 1 µl 32P-UTP, 10 µl ESCs nuclear extract, 10 mM ATP, CTP, GTP, 0.4 mM UTP, 3.2 mM MgCl2. Following indicated time, proteinase K was added to stop transcription. RNA was extracted and run on denaturing polyacrylamide gel and detected by phosphoimager.

CRISPR. The 20nt Guide RNA sequences required for Cas9 specificity were chosen using the online tool at http://crispr.mit.edu/. gRNAs were ordered as custom single stranded DNA oligos (Sigma) with the appropriate reverse sequence and resuspended to 100 µM in dH2O. Complementary oligos were annealed at 100 mM in 10x T4 DNA Ligase Buffer (NEB) by heating to 95C for 2 minutes in a heat block which was subsequently allowed to cool slowly to room temperature. Successful annealing was confirmed by gel electrophoresis and introduced into either the PX461 cloning vectors using Bbs1 (NEB) restriction cloning. For blastocyst injections, Cas9 nickase RNA was used in combination with in vitro transcribed gRNAs and a DNA oligo repair template. gRNA sequence from the PX461 was amplified using oligos

complementary to guide sequence and containing (Sigma) the T7 promoter sequence at the 5' end of the forward primer. PCR was performed using GoTaq 2x Green Master Mix in a 50 ml reaction volume with 200 ng template DNA. PCR thermal programme used was as follows: initial denaturing 95ºC 2mins, then 35x cycles of: second denaturing 95ºC 30 sec, annealing 56ºC 30 sec, extension 72ºC 20 sec, before final extension 72ºC 5 min. PCR product was purified using the PCR purification kit (Qiagen) as per the manufacturer's instructions. A second PCR amplification step was performed using the entire elute from this cleanup of the first PCR reaction using the same thermal cycling profile. RNA synthesis was carried out from the amplified DNA using the MEGAscript T7 Transcription kit (Invitrogen, AM1334) following the manufacturer's instructions. The entire purified PCR product (approximately 1μg) was used with incubation at 37ºC overnight. Transcribed RNA was purified using the RNAeasy kit (Qiagen) following the "cleanup" part of the manufacturer's protocol. RNA was quantified using the Nanodrop, with dilution as appropriate. Injection mixes were prepared in a total volume of 20 μl as follows: Cas9 RNA (TriLink BioTechnologies), 50ng/μl, guide RNAs, 25ng/μl, repair template oligo, 75ng/μl. Multiple oligo repair templates were tried, with silent restriction sites incorporated. Mixes were centrifuged at maximum speed, 4ºC for 30 mins to remove impurities, before the supernatant was transferred to a fresh tube.

RNA isolation and RT-QPCR. RNA was isolated using TRIzol or RNAeasy following the manufacturer's protocol. RNA was then treated with Dnase (Ambion) and transcribed to cDNA using First-Strand Synthesis System from Roche. This was followed by SybrGreen detection system (Lightcycler 2x SybrGreen Mix, Roche).

Immunofluorescence. Cells were seeded on appropriately treated coverslips in 6-well plates. Cells were rinsed in PBS and fixed with 4% paraformaldehyde for 10 minutes at room temperature. The fixed cells were washed with PBS and permabilized using PBS+0.2% Triton. After washing, the slides were blocked in 1% BSA in PBS for 1 hour. Various antibodies were used including: anti-MAP2 (1:200), mouse anti-Tuj1 (1:350), rabbit anti-GFAP (1:200), anti-Nestin, anti-Sox1. Slides were then washed and incubated with the appropriate AlexaFluor- 488 and - 594 labelled secondary antibodies at 1:2000. Final washes were followed by mounting with DAPI vectorshield. A fluorescent upright microscope, Zeiss Axioplan 2 was used to image the cells at 20x magnification.

Networks. The GO network for the genes misregulated in cells harboring slow RNAPII was built using Enrichment Map (Merico et al. 2010) in Cytoscape 3.3.1(Shannon et al. 2003) with the following parameters: p-value cut-off = 0.001; FDR Q value cut-off = 0.01; Jaccard+Overlap Combined option, with cut-off = 0.375; Combined Constant = 0.5. Enriched functional terms were obtained from g:profiler or by GSEA for GO_BP and KEGG pathways. Gorilla, Metascape or g:profiler was employed for the analysis of GO enrichment during neuronal differentiation.

Key reagents table

REAGENT	MANUFACTURER	CATALOG NUMBER
Antibodies		
Tuj1	BioLegend	MMS-435P
Map2	Millipore	MAB3418
GFAP	Sigma-Aldrich	G4546
Rbfox3	Abcam	
Nestin	Abcam	Ab24692
Chemicals		
5,6-dichlorobenzimidazole	Sigma-Aldrich	D1916

1-β-d-ribofuranoside (DRB)		
4-thiouridine	Sigma-Aldrich	T4509
EZ-Link biotin HPDP	Thermo Scientific	21341
Dimethylformamide	Thermo Scientific	20673
No-Weigh dithiothreitol (DTT) microtubes	Thermo Scientific	20291
Cell culture reagents, cytokines		
Recombinant Murine EGF	Peprotech	315-09
Recombinant Human FGF-basic	Peprotech	100-18B
Ascorbic Acid	Stemcell Technologies	07157
Dibutyryl-cAMP	Stemcell Technologies	73886
DMEM/F12	Thermo Scientific	31331028
Neurobasal medium	Thermo Scientific	21103049
GMEM	Thermo Scientific	
MEM Non-essential amino acid		
Sodium pyruvate		
2-mercaptoethanol		
BSA (7.5% solution)	Thermo Scientific	15260037
N-2 Supplement (100x)	Thermo Scientific	17502048
B-27 Supplement (50x)	Thermo Scientific	17504044
PD0325901	Stemcell Technologies	72182
CHIR99021	Miltenyi Biotec	130-103-926
Poly-DL-ornithine hydrobromide,mol wt 3,000-15,000	Sigma-Aldrich	P8638
Commercial Assays and Kits		
RNeasy MinElute clean-up kit	Qiagen	74204
µMacs Streptavidin Kit	Miltenyi	130-074-101
Turbo DNase	Ambion	
NEBNext Ultra II Directional RNA Library Prep Kit for Illumina	Neb	E7420
NEBNext Multiplex Oligos	Neb	E7335, E7500

Acknowledgments

We are grateful to Nick Hastie (MRC HGU) and Wendy Bickmore (MRC HGU) for support at the initial stages of this project. We thank Graeme Grimes (MRC HGU) for help with bioinformatics analysis. We thank Wendy Bickmore (MRC HGU) for critical reading of the manuscript. We acknowledge the contributions of David Read, who recently passed away. This work was supported by Core funding from the Medical Research Council (J.F.C and I.A) and by a Wellcome Trust Investigator Award (Grant 095518/Z/11/Z to J.F.C).

Author contributions

M.M.M., I.R.A and J.F.C. conceived, designed and interpreted the experiments. U.B. and B.J.B. provided bioinformatics analysis and discussion of AS changes during differentiation. S.A contributed to the bioinformatics analysis of RNAPII elongation rates A.R.W., C.H. and F.K. carried out ESCs targeting. The CBS Transgenic Core performed CRISPR injections and mouse work. A.R.K participated in discussions. M.M.M., B.J.B, A.R.K., I.R.A and J.F.C. wrote the paper.

Competing financial interests

The authors declare that they have no competing financial interests

References

Aguirre A, Rubio ME, Gallo V. 2010. Notch and EGFR pathway interaction regulates neural stem cell number and self-renewal. *Nature* **467**: 323–327.

Ahmed K, Dehghani H, Rugg-Gunn P, Fussner E, Rossant J, Bazett-Jones DP. 2010. Global chromatin architecture reflects pluripotency and lineage commitment in the early mouse embryo. *PLoS One* **5**: e10531.

Aitken S, Alexander RD, Beggs JD. 2011. Modelling reveals kinetic advantages of co-transcriptional splicing. ed. R. Guigo. *PLoS Comput Biol* **7**: e1002215.

Alló M, Buggiano V, Fededa JPP, Petrillo E, Schor I, de la Mata M, Agirre E, Plass M, Eyras E, Elela SA, et al. 2009. Control of alternative splicing through siRNA-mediated transcriptional gene silencing. *Nat Struct Mol Biol* **16**: 717–24.

Artus J, Babinet C, Cohen-Tannoudji M. 2006. The cell cycle of early mammalian embryos: lessons from genetic mouse models. *Cell Cycle* **5**: 499–502.

Aslanzadeh V, Huang Y, Sanguinetti G, Beggs JD. 2018. Transcription rate strongly affects splicing fidelity and cotranscriptionality in budding yeast. *Genome Res* **28**: 203–213.

Azuara V, Perry P, Sauer S, Spivakov M, Jørgensen HF, John RM, Gouti M, Casanova M, Warnes G, Merkenschlager M, et al. 2006. Chromatin signatures of pluripotent cell lines. *Nat Cell Biol* **8**: 532–538.

Bentley DL. 2014. Coupling mRNA processing with transcription in time and space. *Nat Rev Genet* **15**: 163–75.

Beyer AL, Osheim YN. 1988. Splice site selection, rate of splicing, and alternative splicing on nascent transcripts. *Genes Dev* **2**: 754–65.

Boireau S, Maiuri P, Basyuk E, de la Mata M, Knezevich A, Pradet-Balade B, Bäcker V, Kornblihtt A, Marcello A, Bertrand E. 2007. The transcriptional cycle of HIV-1 in real-time and live cells. *J Cell Biol* **179**: 291–304.

Bourgeron T. 2015. From the genetic architecture to synaptic plasticity in autism spectrum disorder. *Nat Rev Neurosci* **16**: 551–563.

Buratti E, Baralle FE. 2004. Influence of RNA secondary structure on the pre-mRNA splicing process. *Mol Cell Biol* **24**: 10505–14.

Chanda S, Ang CE, Davila J, Pak C, Mall M, Lee QY, Ahlenius H, Jung SW, Südhof TC, Wernig M. 2014. Generation of induced neuronal cells by the single reprogramming factor ASCL1. *Stem cell reports* **3**: 282–96.

Charizanis K, Lee K-Y, Batra R, Goodwin M, Zhang C, Yuan Y, Shiue L, Cline M, Scotti MM, Xia G, et al. 2012. Muscleblind-like 2-mediated alternative splicing in the developing brain and dysregulation in myotonic dystrophy. *Neuron* **75**: 437–50.

Chen Y, Chafin D, Price DH, Greenleaf AL. 1996. Drosophila RNA polymerase II mutants that affect transcription elongation. *J Biol Chem* **271**: 5993–9.

Conti L, Pollard SM, Gorba T, Reitano E, Toselli M, Biella G, Sun Y, Sanzone S, Ying Q-L, Cattaneo E, et al. 2005. Niche-Independent Symmetrical Self-Renewal of a Mammalian Tissue Stem Cell ed. R. Lovell-Badge. *PLoS Biol* **3**: e283.

Corioni M, Antih N, Tanackovic G, Zavolan M, Krämer A. 2011. Analysis of in situ pre-mRNA targets of human splicing factor SF1 reveals a function in alternative splicing. *Nucleic Acids Res* **39**: 1868–79.

Corvelo A, Hallegger M, Smith CWJ, Eyras E. 2010. Genome-wide association between branch point properties and alternative splicing. *PLoS Comput Biol* **6**: e1001016.

Coulter DE, Greenleaf AL. 1985. A mutation in the largest subunit of RNA polymerase II alters RNA chain elongation in vitro. *J Biol Chem* **260**: 13190–8.

Danko CG, Hah N, Luo X, Martins AL, Core L, Lis JT, Siepel A, Kraus WL. 2013. Signaling pathways differentially affect RNA polymerase II initiation, pausing, and elongation rate in cells. *Mol Cell* **50**: 212–22.

Doe CQ. 2008. Neural stem cells: balancing self-renewal with differentiation. *Development* **135**: 1575–87.

Dujardin G, Lafaille C, de la Mata M, Marasco LE, Muñoz MJ, Le Jossic-Corcos C, Corcos L, Kornblihtt AR. 2014. How Slow RNA Polymerase II Elongation Favors Alternative Exon Skipping. *Mol Cell* **54**: 683–90.

Ehrmann I, Dalgliesh C, Liu Y, Danilenko M, Crosier M, Overman L, Arthur HM, Lindsay S, Clowry GJ, Venables JP, et al. 2013. The tissue-specific RNA binding protein T-STAR controls regional splicing patterns of neurexin pre-mRNAs in the brain. *PLoS Genet* **9**: e1003474.

Eperon LP, Graham IR, Griffiths AD, Eperon IC. 1988. Effects of RNA secondary structure on alternative splicing of pre-mRNA: is folding limited to a region behind the transcribing RNA polymerase? *Cell* **54**: 393–401.

Faigle R, Song H. 2013. Signaling mechanisms regulating adult neural stem cells and neurogenesis. *Biochim Biophys Acta* **1830**: 2435–48.

Fiszbein A, Giono LE, Quaglino A, Berardino BG, Sigaut L, von Bilderling C, Schor IE, Steinberg JH, Rossi M, Pietrasanta LI, et al. 2016. Alternative Splicing of G9a Regulates Neuronal Differentiation. *Cell Rep* **14**: 2797–2808.

Folco EG, Lei H, Hsu JL, Reed R. 2012. Small-scale nuclear extracts for functional assays of gene-expression machineries. *J Vis Exp*.

Fong N, Kim H, Zhou Y, Ji X, Qiu J, Saldi T, Diener K, Jones K, Fu X-D, Bentley DL. 2014. Pre-mRNA splicing is facilitated by an optimal RNA polymerase II elongation rate. *Genes Dev* **28**: 2663–2676.

Fuchs G, Voichek Y, Benjamin S, Gilad S, Amit I, Oren M. 2014. 4sUDRB-seq: measuring genomewide transcriptional elongation rates and initiation frequencies within cells. *Genome Biol* **15**: R69.

Fuchs G, Voichek Y, Rabani M, Benjamin S, Gilad S, Amit I, Oren M. 2015. Simultaneous measurement of genome-wide transcription elongation speeds and rates of RNA polymerase II transition into active elongation with 4sUDRB-seq. *Nat Protoc* **10**: 605–618.

Gabel HW, Kinde B, Stroud H, Gilbert CS, Harmin DA, Kastan NR, Hemberg M, Ebert DH, Greenberg ME. 2015. Disruption of DNA-methylation-dependent long gene repression in Rett syndrome. *Nature* **522**: 89.

Gaspar-Maia A, Alajem A, Meshorer E, Ramalho-Santos M. 2011. Open chromatin in pluripotency and reprogramming. *Nat Rev Mol Cell Biol* **12**: 36–47.

Gavin DP, Grayson DR, Varghese SP, Guizzetti M. 2017. Chromatin Switches during Neural Cell Differentiation and Their Dysregulation by Prenatal Alcohol Exposure. *Genes (Basel)* **8**: 137.

Gkikas D, Tsampoula M, Politis PK. 2017. Nuclear receptors in neural stem/progenitor cell homeostasis. *Cell Mol Life Sci* **74**: 4097–4120.

Goodwin M, Mohan A, Batra R, Lee K-Y, Charizanis K, Gómez FJF, Eddarkaoui S, Sergeant N, Buée L, Kimura T, et al. 2015. MBNL Sequestration by Toxic RNAs and RNA Misprocessing in the Myotonic Dystrophy Brain. *Cell Rep* **12**: 1159–68.

Herzel L, Ottoz DSM, Alpert T, Neugebauer KM. 2017. Splicing and transcription touch base: co-transcriptional spliceosome assembly and function. *Nat Rev Mol Cell Biol* **18**: 637–650.

Ip JY, Schmidt D, Pan Q, Ramani AK, Fraser AG, Odom DT, Blencowe BJ. 2011. Global impact of RNA polymerase II elongation inhibition on alternative splicing regulation. *Genome Res* **21**: 390–401.

Irimia M, Weatheritt RJJ, Ellis JD, Parikshak NNN, Gonatopoulos-Pournatzis T, Babor M, Quesnel-Vallières M, Tapial J, Raj B, O'Hanlon D, et al. 2014. A Highly Conserved Program of Neuronal Microexons Is Misregulated in Autistic Brains. *Cell* **159**: 1511–23.

Jonkers I, Kwak H, Lis JT. 2014. Genome-wide dynamics of Pol II elongation and its interplay with promoter proximal pausing, chromatin, and exons. *Elife* **3**: e02407.

Jonkers I, Lis JT. 2015. Getting up to speed with transcription elongation by RNA polymerase II. *Nat Rev Mol Cell Biol* **16**: 167–177.

King IF, Yandava CN, Mabb AM, Hsiao JS, Huang H-S, Pearson BL, Calabrese JM, Starmer J, Parker JS, Magnuson T, et al. 2013. Topoisomerases facilitate transcription of long genes linked to autism. *Nature* **501**: 58–62.

Koh FM, Lizama CO, Wong P, Hawkins JS, Zovein AC, Ramalho-Santos M. 2015. Emergence of hematopoietic stem and progenitor cells involves a Chd1-dependent increase in total nascent transcription. *Proc Natl Acad Sci U S A* **112**: E1734-43.

de la Mata M, Alonso CR, Kadener S, Fededa JP, Blaustein M, Pelisch F, Cramer P, Bentley D, Kornblihtt AR. 2003. A slow RNA polymerase II affects alternative splicing in vivo. *Mol Cell* **12**: 525–32.

Lagier-Tourenne C, Polymenidou M, Hutt KR, Vu AQ, Baughn M, Huelga SC, Clutario KM, Ling S-C, Liang TY, Mazur C, et al. 2012. Divergent roles of ALS-linked proteins FUS/TLS and TDP-43 intersect in processing long pre-mRNAs. *Nat Neurosci* **15**: 1488–1497.

Langmead B, Trapnell C, Pop M, Salzberg SL. 2009. Ultrafast and memory-efficient alignment of short DNA sequences to the human genome. *Genome Biol* **10**: R25.

Lev Maor G, Yearim A, Ast G. 2015. The alternative role of DNA methylation in splicing regulation. *Trends Genet* **31**: 274–280.

Li Q, Zheng S, Han A, Lin C-H, Stoilov P, Fu X-D, Black DL. 2014. The splicing regulator PTBP2 controls a program of embryonic splicing required for neuronal maturation. *Elife* **3**: e01201.

Licatalosi DD, Mele A, Fak JJ, Ule J, Kayikci M, Chi SW, Clark TA, Schweitzer AC, Blume JE, Wang X, et al. 2008. HITS-CLIP yields genome-wide insights into brain alternative RNA processing. *Nature* **456**: 464–469.

Lienert F, Mohn F, Tiwari VK, Baubec T, Roloff TC, Gaidatzis D, Stadler MB, Schübeler D. 2011. Genomic prevalence of heterochromatic H3K9me2 and transcription do not discriminate pluripotent from terminally differentiated cells. ed. W. Reik. *PLoS Genet* **7**: e1002090.

Lin S, Coutinho-Mansfield G, Wang D, Pandit S, Fu X-D. 2008. The splicing factor SC35 has an active role in transcriptional elongation. *Nat Struct Mol Biol* **15**: 819–26.

Lovci MT, Ghanem D, Marr H, Arnold J, Gee S, Parra M, Liang TY, Stark TJ, Gehman LT, Hoon S, et al. 2013. Rbfox proteins regulate alternative mRNA splicing through evolutionarily conserved RNA bridges. *Nat Struct Mol Biol* **20**: 1434–1442.

Martinez FJ, Pratt GA, Van Nostrand EL, Batra R, Huelga SC, Kapeli K, Freese P, Chun SJ, Ling K, Gelboin-Burkhart C, et al. 2016. Protein-RNA Networks Regulated by Normal and ALS-Associated Mutant HNRNPA2B1 in the Nervous System. *Neuron* **92**: 780–795.

Merico D, Isserlin R, Stueker O, Emili A, Bader GD. 2010. Enrichment map: a network-based method for gene-set enrichment visualization and interpretation. *PLoS One* **5**: e13984.

Meshorer E, Yellajoshula D, George E, Scambler PJ, Brown DT, Misteli T. 2006. Hyperdynamic Plasticity of Chromatin Proteins in Pluripotent Embryonic Stem Cells. *Dev Cell* **10**: 105–116.

Mortin MA, Kim WJ, Huang J. 1988. Antagonistic interactions between alleles of the RpII215 locus in Drosophila melanogaster. *Genetics* **119**: 863–73.

Muñoz MJ, Pérez Santangelo MS, Paronetto MP, de la Mata M, Pelisch F, Boireau S, Glover-Cutter K, Ben-Dov C, Blaustein M, Lozano JJ, et al. 2009. DNA damage regulates alternative splicing through inhibition of RNA polymerase II elongation. *Cell* **137**: 708–20.

Naftelberg S, Schor IE, Ast G, Kornblihtt AR. 2015. Regulation of Alternative Splicing Through Coupling with Transcription and Chromatin Structure. *Annu Rev Biochem* **84**: 165–198.

Pandya-Jones A, Black DL. 2009. Co-transcriptional splicing of constitutive and alternative exons. *RNA* **15**: 1896–908.

Patton JG, Porro EB, Galceran J, Tempst P, Nadal-Ginard B. 1993. Cloning and characterization of PSF, a novel pre-mRNA splicing factor. *Genes Dev* **7**: 393–406.

Percharde M, Wong P, Ramalho-Santos M. 2017. Global Hypertranscription in the Mouse Embryonic Germline. *Cell Rep* **19**: 1987–1996.

Poulos MG, Batra R, Li M, Yuan Y, Zhang C, Darnell RB, Swanson MS. 2013. Progressive impairment of muscle regeneration in muscleblind-like 3 isoform knockout mice. *Hum Mol Genet* **22**: 3547–58.

Rädle B, Rutkowski AJ, Ruzsics Z, Friedel CC, Koszinowski UH, Dölken L. 2013. Metabolic Labeling of Newly Transcribed RNA for High Resolution Gene Expression Profiling of RNA Synthesis, Processing and Decay in Cell Culture. *J Vis Exp* e50195–e50195.

Raj B, Irimia M, Braunschweig U, Sterne-Weiler T, O'Hanlon D, Lin Z-Y, Chen GI, Easton LE, Ule J, Gingras A-C, et al. 2014. A global regulatory mechanism for activating an exon network required for neurogenesis. *Mol Cell* **56**: 90–103.

Ray D, Kazan H, Cook KB, Weirauch MT, Najafabadi HS, Li X, Gueroussov S, Albu M, Zheng H, Yang A, et al. 2013. A compendium of RNA-binding motifs for decoding gene regulation. *Nature* **499**: 172–177.

Roberts GC, Gooding C, Mak HY, Proudfoot NJ, Smith CW. 1998. Co-transcriptional commitment to alternative splice site selection. *Nucleic Acids Res* **26**: 5568–72.

De Rubeis S, He X, Goldberg AP, Poultney CS, Samocha K, Ercument Cicek A, Kou Y, Liu L, Fromer M, Walker S, et al. 2014. Synaptic, transcriptional and chromatin genes disrupted in autism. *Nature* **515**: 209–215.

Saldi T, Fong N, Bentley DL. 2018. Transcription elongation rate affects nascent histone pre-mRNA folding and 3′ end processing. *Genes Dev* **32**: 297–308.

Sanchez-Alvarez M, Goldstrohm AC, Garcia-Blanco MA, Sune C. 2006. Human Transcription Elongation Factor CA150 Localizes to Splicing Factor-Rich Nuclear Speckles and Assembles Transcription and Splicing Components into Complexes through Its Amino and Carboxyl Regions. *Mol Cell Biol* **26**: 4998–5014.

Schor IE, Rascovan N, Pelisch F, Alló M, Kornblihtt AR. 2009. Neuronal cell depolarization induces intragenic chromatin modifications affecting NCAM alternative splicing. *Proc Natl Acad Sci U S A* **106**: 4325–30.

Schreiner D, Nguyen T-M, Russo G, Heber S, Patrignani A, Ahrné E, Scheiffele P. 2014. Targeted combinatorial alternative splicing generates brain region-specific repertoires of neurexins. *Neuron* **84**: 386–98.

Schwartz S, Ast G. 2010. Chromatin density and splicing destiny: on the cross-talk between chromatin structure and splicing. *EMBO J* **29**: 1629–36.

Selth LA, Sigurdsson S, Svejstrup JQ. 2010. Transcript Elongation by RNA Polymerase II. *Annu Rev Biochem* **79**: 271–93.

Shannon P, Markiel A, Ozier O, Baliga NS, Wang JT, Ramage D, Amin N, Schwikowski B, Ideker T. 2003. Cytoscape: a software environment for integrated models of biomolecular interaction networks. *Genome Res* **13**: 2498–504.

Singh J, Padgett RA. 2009. Rates of in situ transcription and splicing in large human genes. *Nat Struct Mol Biol* **16**: 1128–33.

Suñé C, Garcia-Blanco MA. 1999. Transcriptional cofactor CA150 regulates RNA polymerase II elongation in a TATA-box-dependent manner. *Mol Cell Biol* **19**: 4719–28.

Takahashi T, Nowakowski RS, Caviness VS. 1995. The cell cycle of the pseudostratified ventricular epithelium of the embryonic murine cerebral wall. *J Neurosci* **15**: 6046–57.

Takeuchi A, Iida K, Tsubota T, Hosokawa M, Denawa M, Brown JB, Ninomiya K, Ito M, Kimura H, Abe T, et al. 2018. Loss of Sfpq Causes Long-Gene Transcriptopathy in the Brain. *Cell Rep* **23**: 1326–1341.

Tapial J, Ha KCH, Sterne-Weiler T, Gohr A, Braunschweig U, Hermoso-Pulido A, Quesnel-Vallières M, Permanyer J, Sodaei R, Marquez Y, et al. 2017. An atlas of alternative splicing profiles and functional associations reveals new regulatory programs and genes that simultaneously express multiple major isoforms. *Genome Res* **27**: 1759–1768.

Thomas L, Hartung K, Langosch D, Rehm H, Bamberg E, Franke W, Betz H. 1988. Identification of synaptophysin as a hexameric channel protein of the synaptic vesicle membrane. *Science (80-)* **242**: 1050–1053.

Ule J, Stefani G, Mele A, Ruggiu M, Wang X, Taneri B, Gaasterland T, Blencowe BJ, Darnell RB. 2006. An RNA map predicting Nova-dependent splicing regulation. *Nature* **444**: 580–586.

Veloso A, Kirkconnell KS, Magnuson B, Biewen B, Paulsen MT, Wilson TE, Ljungman M. 2014. Rate of elongation by RNA polymerase II is associated with specific gene features and epigenetic modifications. *Genome Res* **24**: 896–905.

Wen B, Wu H, Shinkai Y, Irizarry RA, Feinberg AP. 2009. Large histone H3 lysine 9 dimethylated chromatin blocks distinguish differentiated from embryonic stem cells. *Nat Genet* **41**: 246–50.

Williamson L, Saponaro M, Boeing S, East P, Mitter R, Kantidakis T, Kelly GP, Lobley A, Walker J, Spencer-Dene B, et al. 2017. UV Irradiation Induces a Non-coding RNA that Functionally Opposes the Protein Encoded by the Same Gene. *Cell* **168**: 843–855.e13.

Yeo G, Burge CB. 2004. Maximum entropy modeling of short sequence motifs with applications to RNA splicing signals. *J Comput Biol* **11**: 377–94.

Ying Q-L, Stavridis M, Griffiths D, Li M, Smith A. 2003. Conversion of embryonic stem cells into neuroectodermal precursors in adherent monoculture. *Nat Biotechnol* **21**: 183–6.

Yoon K-J, Vissers C, Ming G-L, Song H. 2018. Epigenetics and epitranscriptomics in temporal patterning of cortical neural progenitor competence. *J Cell Biol* **217**: 1901–1914.

Zhang C, Frias MA, Mele A, Ruggiu M, Eom T, Marney CB, Wang H, Licatalosi DD, Fak JJ, Darnell RB. 2010. Integrative modeling defines the Nova splicing-regulatory network and its combinatorial controls. *Science* **329**: 439–43.

Zhang C, Zhang Z, Castle J, Sun S, Johnson J, Krainer AR, Zhang MQ. 2008. Defining the regulatory network of the tissue-specific splicing factors Fox-1 and Fox-2. *Genes Dev* **22**: 2550–63.

Figure 1 Generation of slow RNAPII knock-in mutant mouse ESCs. (**a**) Cartoon depicting the mutagenesis strategy, including the genomic target locus, as well as the structure of targeting vector. (**b**) Sequencing of cDNA confirms the presence of the R749H mutation. (**c**) Restriction enzyme diagnostic test for the presence of the R749H mutation.

Figure 2 CRISPR/Cas-mediated generation of a slow RNAPII knock-in mutant mouse. (**a**) Cartoon depicting the mutagenesis strategy, including the genomic target locus, as well as two repair templates, either introducing a silent mutation (silent oligo) or the R749H mutation (slow oligo). Multiple repair oligo templates were tested with different composition of silent restriction sites. (**b**) Number of WT, heterozygous and homozygous embryos (E3.5 and E9.5), as well as born mice from several targeting experiments introducing either the slow (R749H) RNAPII mutation or repaired with the WT sequence.

Figure 3 Global analysis of transcription elongation rate in mouse ESCs by 4sU-DRBseq. (**a**) Schematic of the 4sU-DRB-seq labeling protocol. (**b**) Meta-gene profile of normalized 4sU-DRB-seq reads in WT/WT and slow/slow ESCs. (**c-d**) Density and box plot of elongation rate (bases/min) calculated for genes common in all genotypes in WT/WT, WT/slow and slow/slow ESCs. Box and whisker (5-95 percentile) indicates median. Mann-Whitney test, $p < 0.0001$.

Figure 4 (**a**) Schematic of the neural differentiation system used in this study. (**b-e**) Immunofluorescence or brightfield images of different stages of neural differentiation. White arrows indicate NSCs and green arrows differentiated cells.

Figure 5 The rate of transcriptional elongation influences AS decisions in ESCs and during neural differentiation. (**a**) Number of AS events that are sensitive to a slow elongation rate, including cassette exons, microexons, alternative 3' or 5' splice sites and retained introns in ESCs and at different stages of neural differentiation. UP and DOWN refers to increased or decreased levels of a splicing event in slow/slow cells relative to WT cells. Only events that are significantly different (FDR<0.05) with dPSI (percent spliced in) ≥10% were considered. (**b**) RT-PCR analysis validation of selected alternatively spliced exons. RT PCR was performed on total RNA from WT or slow/slow ESCs, NPCs or neurons. PCR products were visualised and quantified by Bioanalyzer (Agilent). (**c**) Length of alternative exons and flanking introns in ESCs and neurons. Box and whisker (5-95 percentile) indicates median. Mann-Whitney test, $p < 0.01$ (*), 0.001 (**), 0.0001 (***).

Figure 6 A reduced transcriptional elongation results in gross changes in gene expression during neural differentiation. ((**a**) MA plots for pluripotent ESCs and all stages of neural differentiation. The y-axis depicts the $\log_2$ fold change in gene expression in slow/slow cells (M), as compared to WT, whereas the x-axis is the log of average mean read count for each gene between all samples. Each dot represents one gene. Red dots depict genes with significantly altered expression values (Benjamini and Hochberg (B + H) adjusted *p* value <0.01), with mean expression of at least RPKM=5. Grey line depicts fold change (FC) of either two-fold upregulation or

downregulation. (**b**) number of upregulated and downregulated genes in ESCs and at different stages of neural differentiation.

Figure 7 A slow RNAPII preferentially affects synaptic genes. (**a**) Cytoscape-generated enrichment map, visualizing the results of gene-sets enrichment for genes downregulated and differentially spliced in slow/slow neurons as a network, where nodes represent the gene-sets, and edges their similarity. (**b**) Bar plot showing misregulation of neuron-specific AS in slow/slow cells. Red and blue represent events normally upregulated (neural- high) or downregulated (neural- low) in WT neurons. Numbers in the bars represent number of events that change in slow/slow neurons as compared to WT neurons and that overlap with neural-specific events. CE, cassette exons; MIC, microexons; Alt3/5, alternative 3'/5' splice site; IR, intron retention. (**c**) Cartoon representation of alternatively spliced genes involved in synapse signaling and axonal transport. (**d**) Box plot showing the length of upregulated, downregulated, not affected genes, not affected genes only expressed in neurons (but not in ESCs), as well as length of pre-mRNAs affected by AS (AE, for Alternative exons) or included in the network shown in Fig. 7A. (**e**) Percentage of genes that are downregulated in neurons; plotted as a sliding window of 100 genes by length.

Figure 1

a

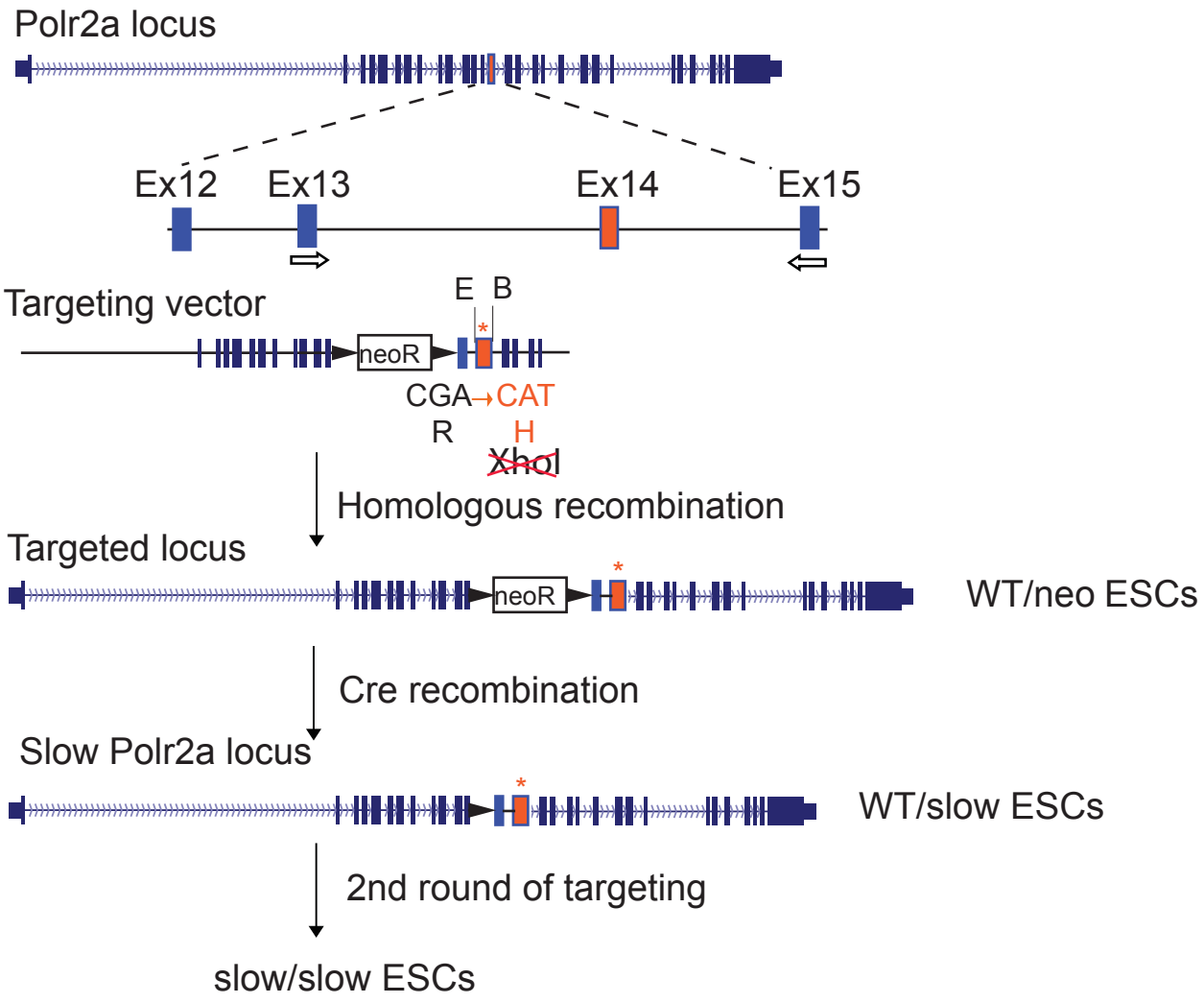
Polr2a locus
Ex12
Ex13
Ex14
Ex15
Targeting vector
E
B
neoR
CGA→CAT
R
H
XhoI
Homologous recombination
Targeted locus
neoR
WT/neo ESCs
Cre recombination
Slow Polr2a locus
WT/slow ESCs
2nd round of targeting
slow/slow ESCs

b

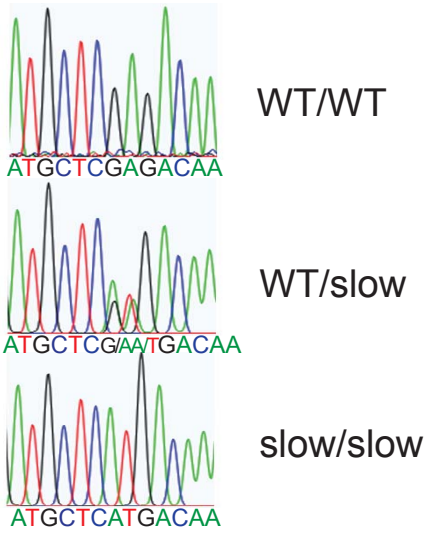
ATGCTCGAGACAA
WT/WT
ATGCTCGAATGACAA
WT/slow
ATGCTCATGACAA
slow/slow

c

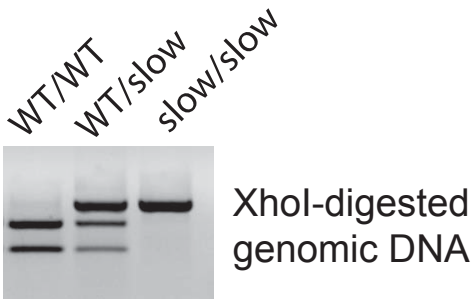
WT/WT
WT/slow
slow/slow
XhoI-digested
genomic DNA

Figure 2

a

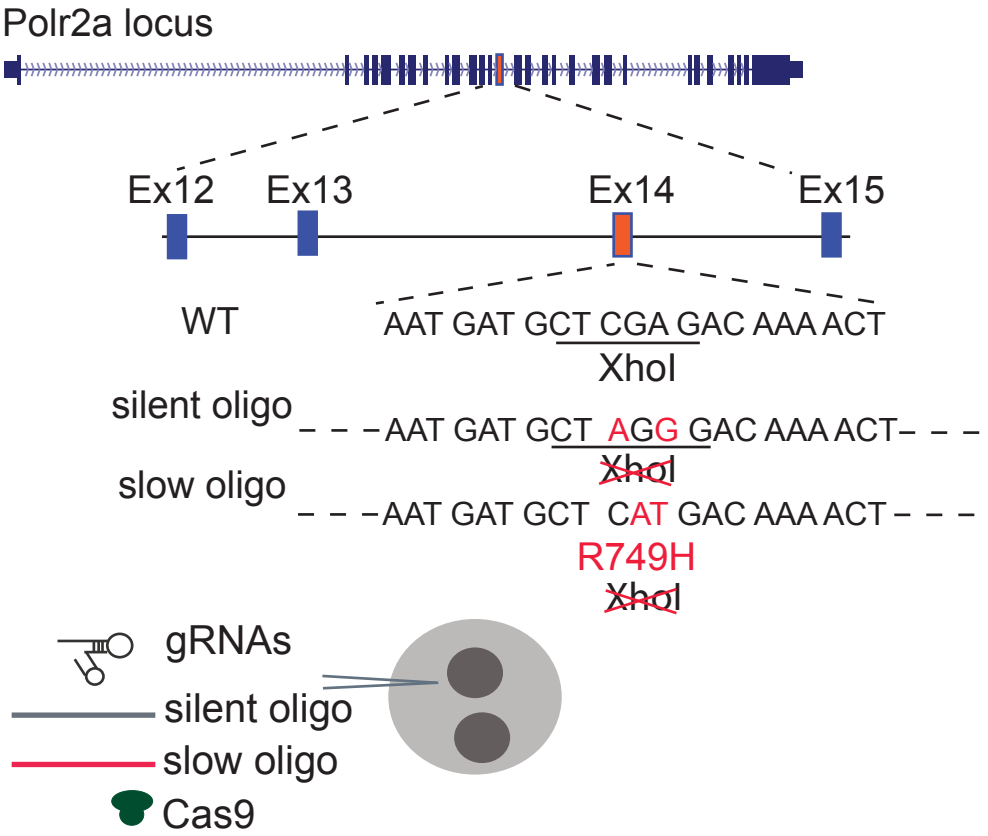

b

	Genotype	E3.5	E9.5	Born
WT mice	WT/WT*	120	64	92
	WT/silent oligo	7	9	4
	silent oligo/silent oligo	4	10	2
Slow hets	WT/slow	32	1	0
	silent oligo/slow	0	0	0
Slow homozyg	slow/slow	1	0	0

Figure 3

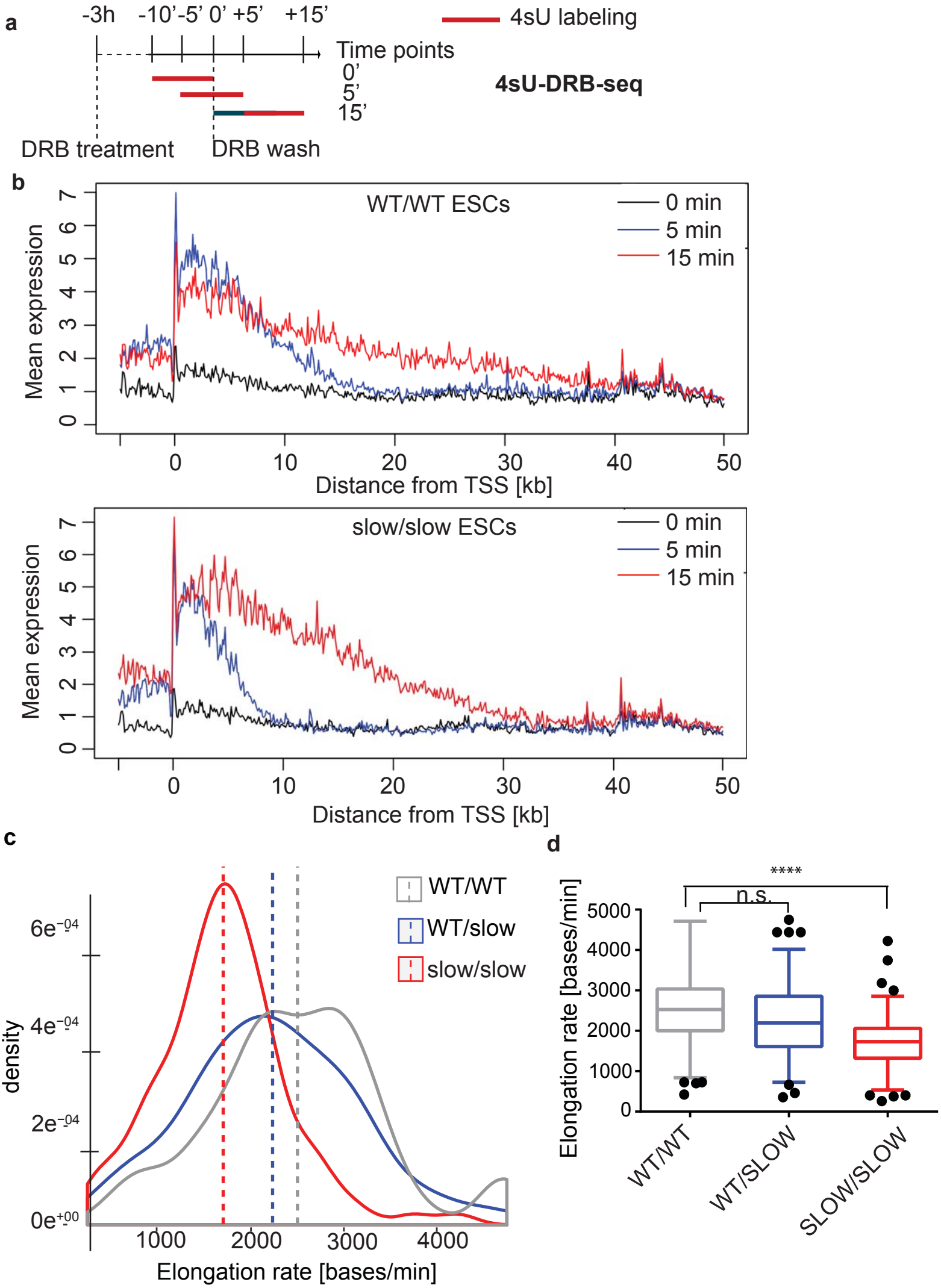
a
-3h
-10'-5' 0' +5'
+15'
4sU labeling
Time points
0'
5'
15'
4sU-DRB-seq
DRB treatment
DRB wash
b
WT/WT ESCs
0 min
5 min
15 min
Mean expression
Distance from TSS [kb]
slow/slow ESCs
0 min
5 min
15 min
Mean expression
Distance from TSS [kb]
c
WT/WT
WT/slow
slow/slow
density
Elongation rate [bases/min]
d
****
n.s.
Elongation rate [bases/min]
WT/WT
WT/SLOW
SLOW/SLOW

Figure 4

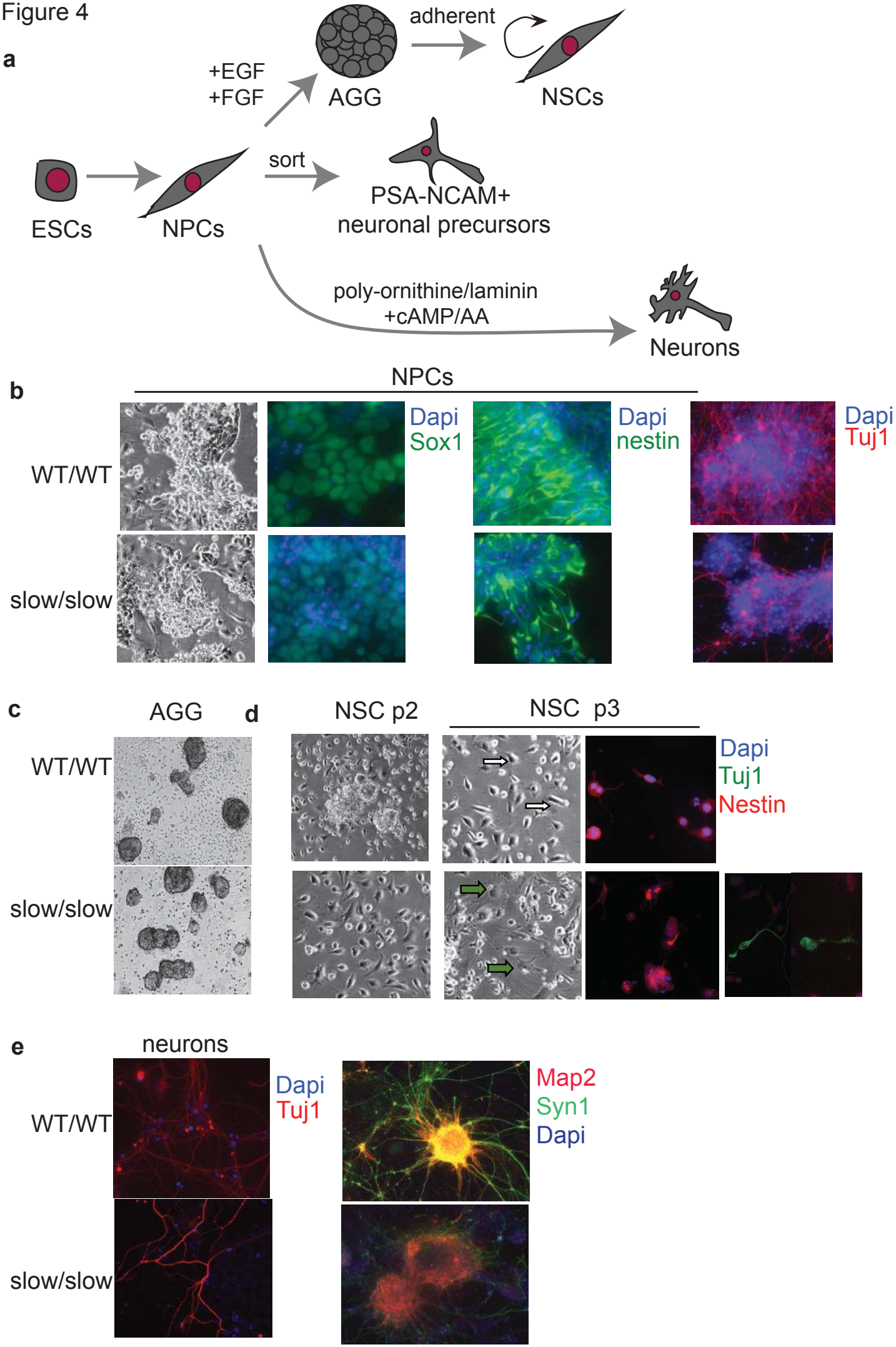
a
adherent
+EGF
+FGF
AGG
NSCs
sort
ESCs
NPCs
PSA-NCAM+
neuronal precursors
poly-ornithine/laminin
+cAMP/AA
Neurons
b
NPCs
WT/WT
slow/slow
Dapi
Sox1
Dapi
nestin
Dapi
Tuj1
c
AGG
d
NSC p2
NSC p3
WT/WT
slow/slow
Dapi
Tuj1
Nestin
e
neurons
WT/WT
slow/slow
Dapi
Tuj1
Map2
Syn1
Dapi

Figure 5

a

	ESCs		NPCs		PSA-NCAM+		Neurons	
	UP	DOWN	UP	DOWN	UP	DOWN	UP	DOWN
Cassette exon	78	84	164	487	47	137	411	225
Microexon	2	10	7	37	3	11	13	55
Alternative 3'/5' splice site	11	9	90	64	14	18	30	41
Intron retention	51	13	175	106	63	16	136	109

b (i) ESCs (iii) Neurons

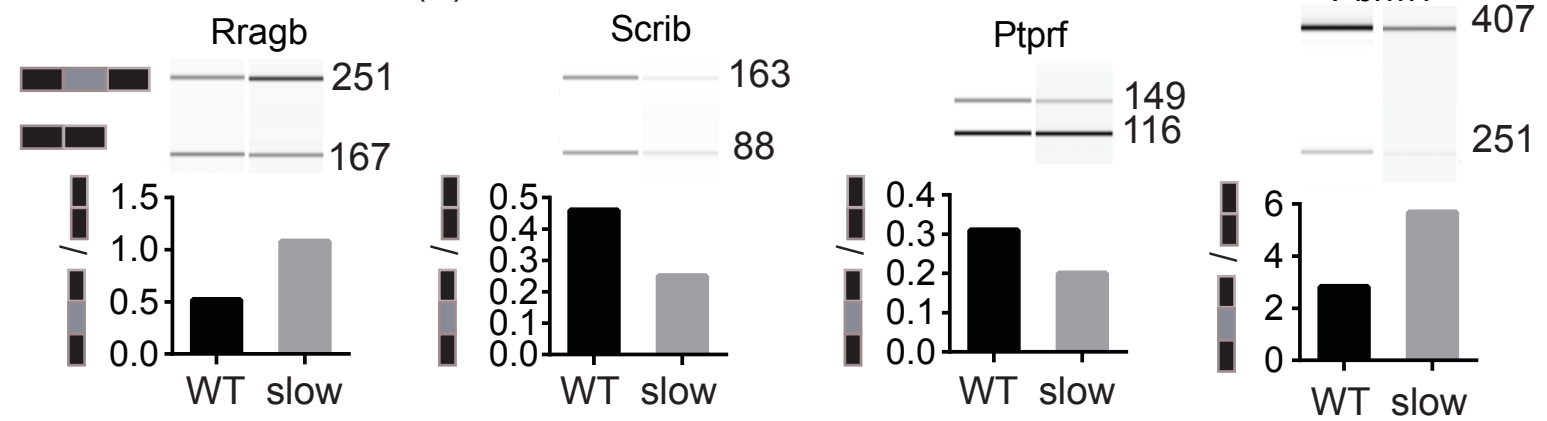

(ii) NPCs

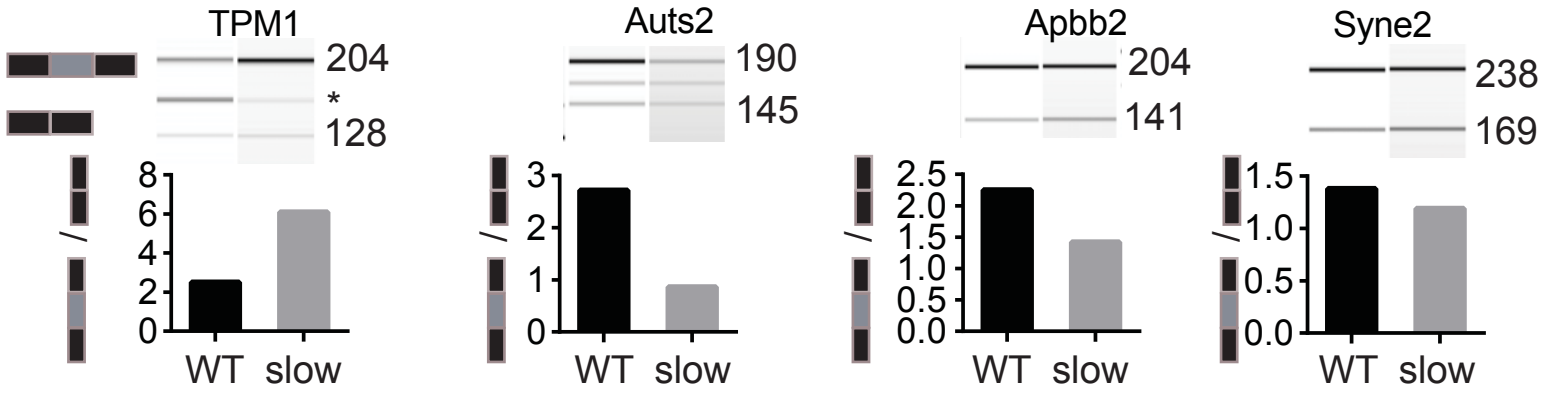

c

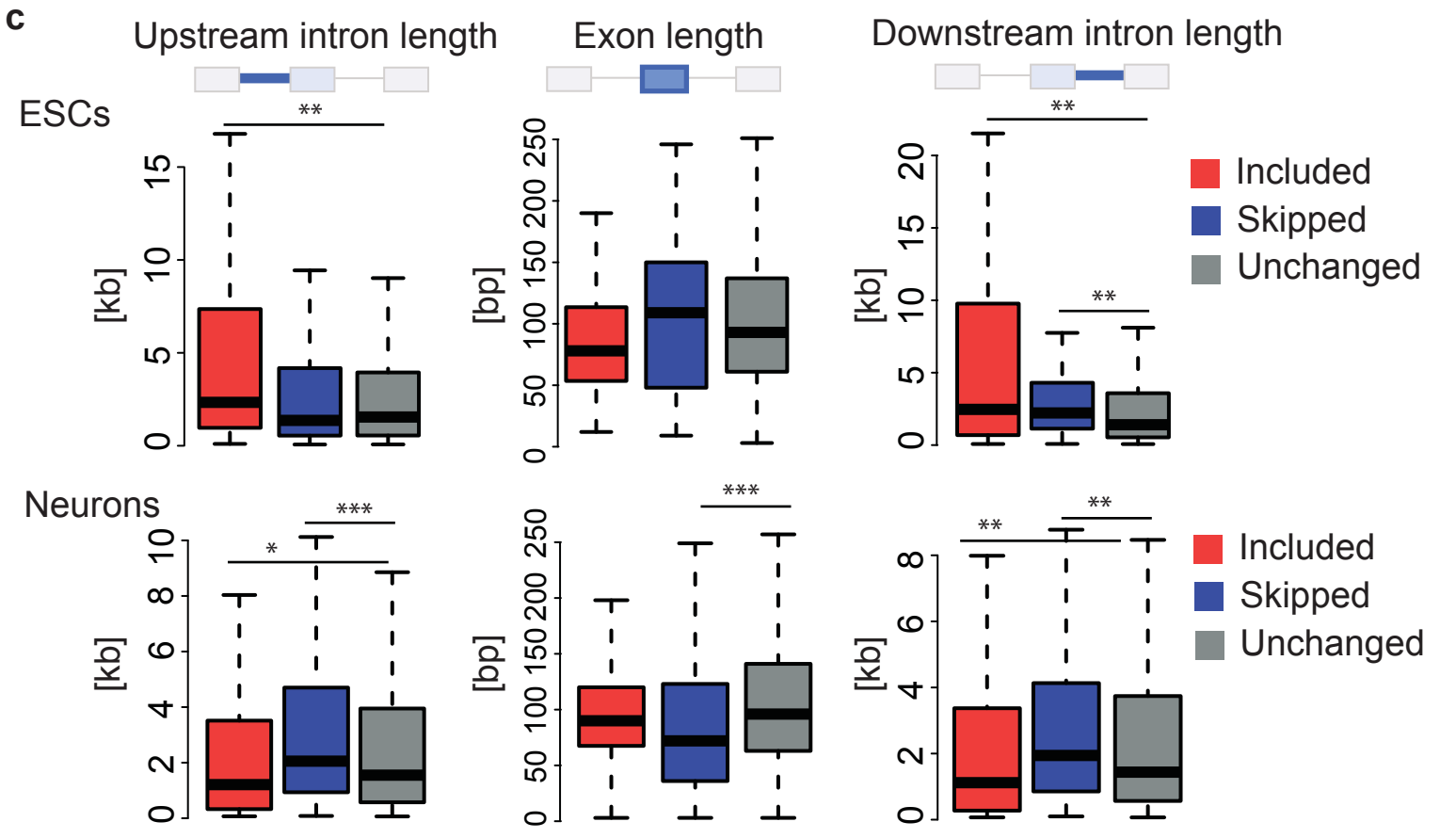

Figure 6

a

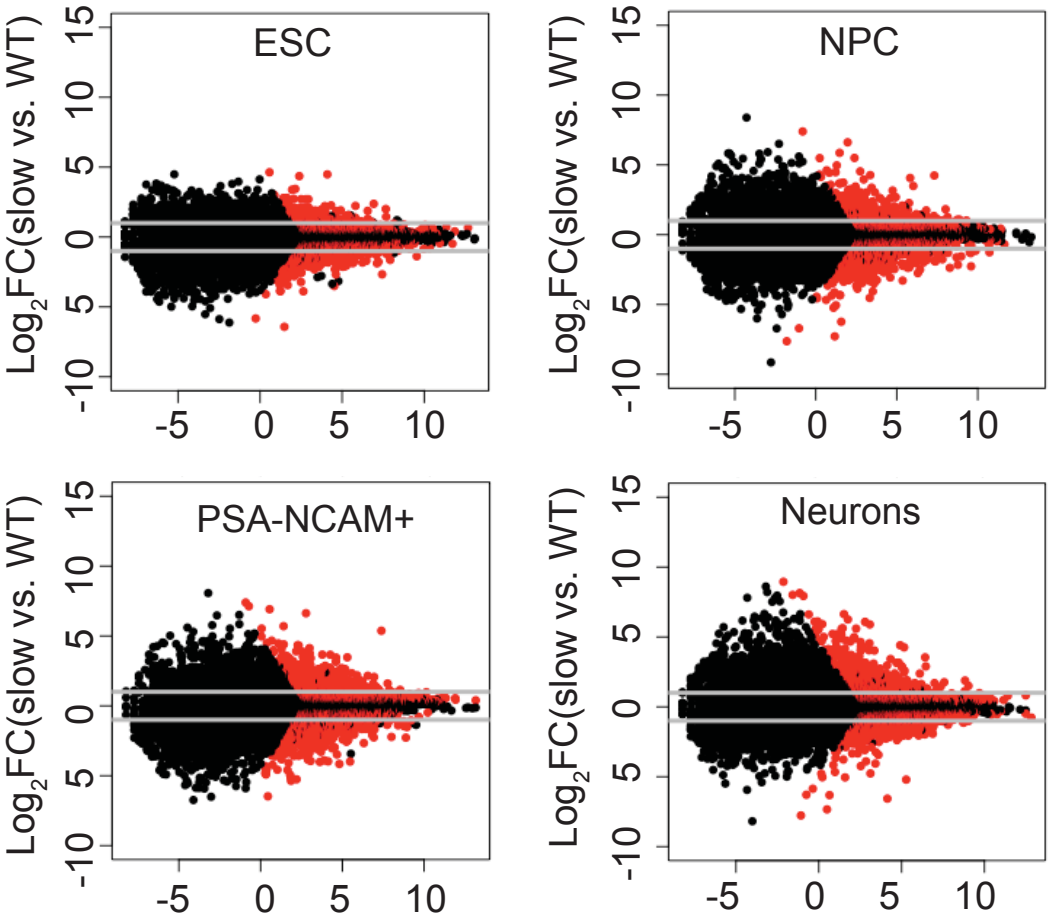

b

	ESC	NPC	PSA-NCAM+	Neurons
UP	78	84	164	487
DOWN	2	10	7	37

Figure 7

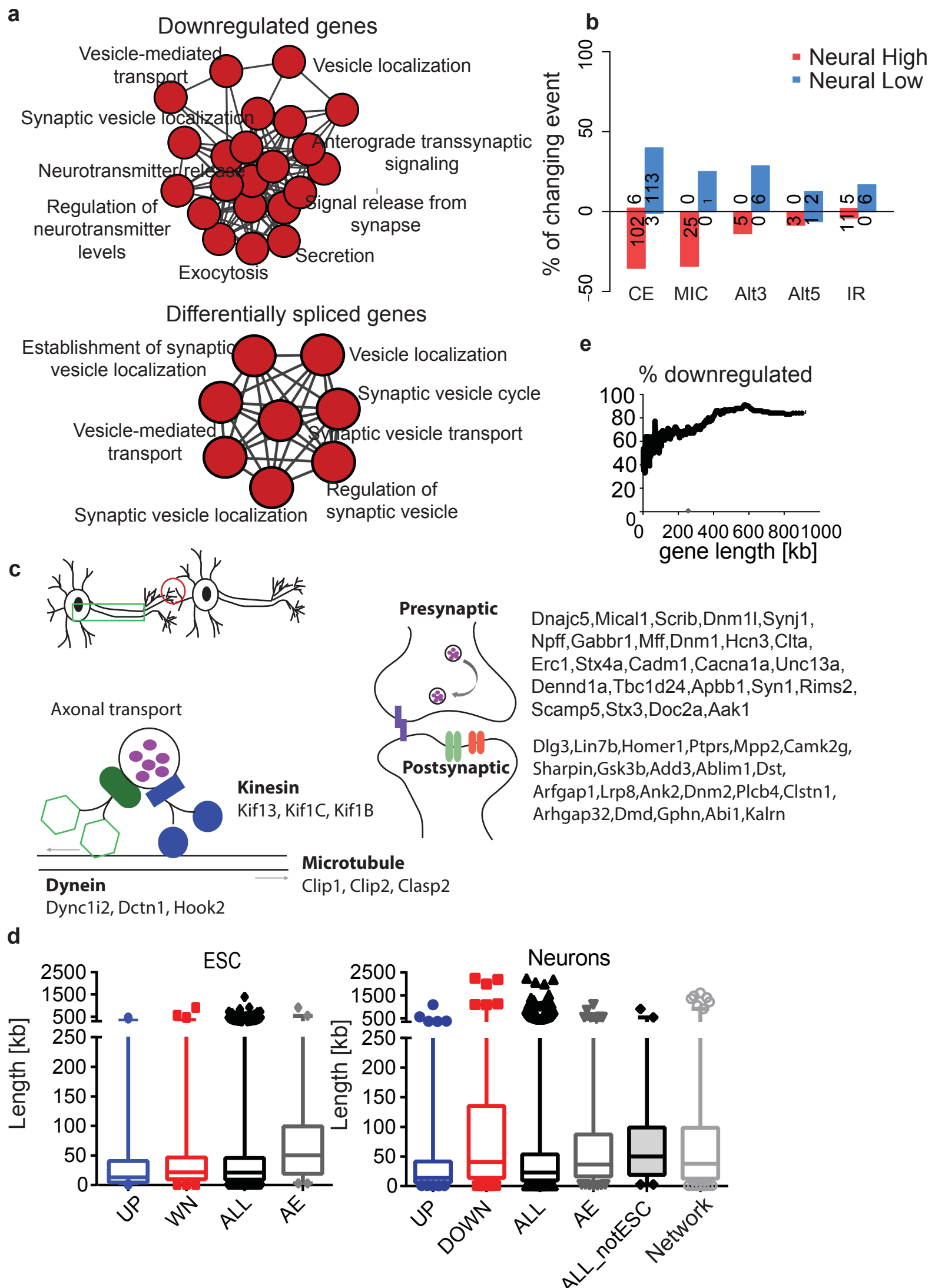
a
Downregulated genes
Vesicle-mediated transport
Vesicle localization
Synaptic vesicle localization
Anterograde transsynaptic signaling
Neurotransmitter release
Regulation of neurotransmitter levels
Signal release from synapse
Secretion
Exocytosis
Differentially spliced genes
Establishment of synaptic vesicle localization
Vesicle localization
Synaptic vesicle cycle
Vesicle-mediated transport
Synaptic vesicle transport
Regulation of synaptic vesicle
Synaptic vesicle localization
b
Neural High
Neural Low
% of changing event
100
50
0
-50
CE
MIC
Alt3
Alt5
IR
e
% downregulated
100
80
60
40
20
0
0
200 400 600 800 1000
gene length [kb]
c
Presynaptic
Postsynaptic
Dnajc5,Mical1,Scrib,Dnm1l,Synj1,
Npff,Gabbr1,Mff,Dnm1,Hcn3,Clta,
Erc1,Stx4a,Cadm1,Cacna1a,Unc13a,
Dennd1a,Tbc1d24,Apbb1,Syn1,Rims2,
Scamp5,Stx3,Doc2a,Aak1
Dlg3,Lin7b,Homer1,Ptprs,Mpp2,Camk2g,
Sharpin,Gsk3b,Add3,Ablim1,Dst,
Arfgap1,Lrp8,Ank2,Dnm2,Plcb4,Clstn1,
Arhgap32,Dmd,Gphn,Abi1,Kalrn
Axonal transport
Kinesin
Kif13, Kif1C, Kif1B
Microtubule
Clip1, Clip2, Clasp2
Dynein
Dync1i2, Dctn1, Hook2
d
ESC
Neurons
Length [kb]
2500
1500
500
250
200
150
100
50
0
UP
WN
ALL
AE
DOWN
ALL_notESC
Network

Gene	Exon	AS	Protein change	Protein/Isoform function	Disease
Kif1b	Ex27	Skipped	no PH domain-like, aa change in GTPase domain	long isoform transports synaptic vesicle precursors	Charcot–Marie–Tooth Disease Type 2A
Scrib	Ex36	Skipped	Shorter protein lacking Discs domain	scaffolding protein, key role for neurotransmitter release	ASD, ADHD, microcephaly
Apbb1	MIC /Ex9	Skipped	Inclusion enhances interaction with Kat5, but not APP	neuronal positioning and axon outgrowth, synaptic vesicle loading	ASD,Alzheimer's disease
Dnm1	Ex10	Included	aa substitution in dynamin domain	activity-dependent synaptic vesicle endocytosis and membrane recycling	epileptic encephalopathy, Lennox-Gastaut Syndrome
Dlg3	Ex7	Included	shorter protein lacking Discs large domain	regulates cortical synapse development	ASD,non-syndromic mental retardation
Syn1	Intron retention			synaptic vesicle release, establishes synaptic vesicle reserve pool	ASD, epilepsy
Gabbr1	Intron retention		ORF disruption upon sequence inclusion	GABA receptor	ASD, Schizophrenia

Table 1. Examples of AS events presented in Figure 7C